THE INFLUENCE OF INHERITED STRUCTURES ON SEGMENTATION AND LINKAGES OF TWO SUBPARALLEL FAULTS IN SOUTHERN MALAWI RIFT

By

STEVEN JOHNSON

Bachelor of Science in Geology

Oklahoma State University

Stillwater, Oklahoma

2016

Submitted to the Faculty of the
Graduate College of the
Oklahoma State University
in partial fulfillment of
the requirements for
the Degree of
MASTER OF SCIENCE
May, 2018

THE INFLUENCE OF INHERITED STRUCTURES ON SEGMENTATION AND LINKAGES OF TWO SUBPARALLEL FAULTS IN SOUTHERN MALAWI RIFT

Thesis Approved:

Dr. Daniel Laó Dávila

Thesis Adviser

Dr. Mohamed Abdelsalam

Dr. Estella Atekwana

.

ACKNOWLEDGEMENTS

The aeromagnetic data was provided by the Geological Survey of Malawi Department. A special thanks to Jalf Salima and Patrick Chindandali of the Geological Survey of Malawi Department for their support and cooperation during the fieldwork. We would like to thank our 2017 NSF-IRES participants Emily Elifritz, Kimberly Méndez-Méndez, William Mynatt, and Stephen Beresh. Leonard Kalindekafe, Chikondi Chisenga, Steven Gondwe, Mathew Mkumbura, and Dickson Kalaguluka of the Malawi University of Science and Technology are acknowledged for their assistance collecting field data. Thanks to Liang Xue, Victor Nyalugwe, Micah Mayle, and Folarin Kolawole for their help with data processing and general input. Thank you to Inés Barrios Galíndez, Nathan Campbell, Brandon Chase, Estefanny Dávalos- Elizondo, Tadesse Alemu, Luelseged Emishaw, and Dr. Andrew Katumwehe for their help and expertise and general support during this research mission. I would also like to thank my advisor Dr. Laó Dávila and committee Dr. Mohamed Abdelsalam and Dr. Estella Atekwana for their contributions, help, insight, and expertise which made this research possible. This research was supported by the National Science Foundation Grant No. II-1358150.

Name: Steven Johnson

Date of Degree: MAY, 2018

Title of Study: THE INFLUENCE OF INHERITED STRUCTURES ON SEGMENTATION AND LINKAGE OF TWO SUB PARALLEL FAULTS IN SOUTHERN MALAWI RIFT

Major Field: GEOLOGY

Abstract:

Important questions remain about the role preexisting structures play on the development of magma poor rifts. The influence of preexisting pervasive upper crustal fabrics on the development and evolution of faults is poorly understood. In Malawi two large (>100 km) synthetic normal faults the Chirobwe-Ncheu and Bilila-Mtakataka faults, were analyzed for the effect of pervasive fabrics on fault segment and linkage. We used Shuttle RADAR Topography Mission Digital Elevation Models (SRTM DEM) and high resolution aeromagnetic data to determine fault segmentation from both topographic displacement profiles and Source Parameter Imaging (SPI) depths. Moreover, the combination of SRTM DEM and aeromagnetic data allowed for the delineation of the upper crustal pervasive fabrics. Our results show that each fault is broadly composed of three segments. The location and orientation of the fault segments are affected by the gneissic fabrics where the foliations are perpendicular to extension direction. Furthermore the combination of the regional joints and the gneissic fabrics control the geometry of the linkage zones. The lengths and segmentation for each of these faults established by this study have an important relationship to the seismic hazard for the region. Finally, our research shows that the faults exhibit characteristics of two models of fault growth where the type of growth is modulated by the pervasive upper crustal inherited fabrics. Therefore, our work demonstrates the effects that preexisting pervasive fabrics may exert on the development, evolution, and linkage of segments in two large faults in a magma poor rift.

TABLE OF CONTENTS

LIST OF TABLES

LIST OF FIGURES

Figure Page

CHAPTER I

INTRODUCTION

An important question in tectonics is, how crustal fault networks evolve within continental rifts. Specifically, how faults in continental rifts evolve without a significant contribution of magma to the thinning of lithosphere (Dunbar & Sawyer, 1989; Kendall & Lithgow-Bertelloni, 2016). In magma-poor continental rifts, such as the Western Branch of the East African Rift System (EARS), previous studies suggest that pre-existing structures play a significant role in rift evolution (e.g. Daly et al., 1989; Versfelt & Rosendahl, 1989; Fossen et al., 2000; Morley, 2010; Katumwehe et al., 2015; Fossen & Rotevatn, 2016). Lithospheric structures such as mobile belts and discrete structures like preexisting suture zones, shear zones, or faults are known to facilitate strain localization (e.g. McConnell 1972; Daly et al., 1989; Holdsworth et al., 1997; Chorowicz, 2005; Misra & Mukherjee 2015; Phillips et al., 2016; Dawson et al., 2018; Kolawole et al., 2018). Even within individual magma-poor rifts, discrete inherited structures have been suggested as the cause for rift scale segmentation and geometry (Ring, 1994; Aanyu & Koehn 2011; Laó-Dávila et al., 2015; Mortimer et al., 2016; Kolawole et al. 2018).

The effect of penetrative or pervasive inherited upper crustal fabrics (i.e. closely spaced small structures found throughout a region) on the development and evolution of faults has been demonstrated in models (e.g. Morley 1999; Corti et al., 2007; Henza et al., 2011; Chattopadhyay

& Chakra 2013; Misra & Mukherjee 2015; Zwaan et al., 2016; Zwaan & Schreurs 2017). Analog modeling has shown that favorably-oriented weak structures (i.e. strike perpendicular to minimum compressive stress) preferentially accommodate slip or are reactivated instead of forming new faults (Corti 2012; Chattopadhyay & Chakra 2013; Zwaan & Schreurs 2017). Furthermore, studies have demonstrated that pervasive inherited weak fabrics oblique to extension by as much as 45-60° may still accommodate slip (Morley et al., 2004; Chattopadhyay & Chakra 2013; Zwaan et al., 2016). Additionally, in terrains with pervasive fabric, the local maximum horizontal stress may be reoriented due to the strength anisotropy of gneissic foliations producing oblique faulting and linkages that develop with the same strike as the preexisting fabric (Morley et al., 2004; Morley, 2010; Zwaan & Schreurs 2017). Examples of these processes in natural field settings have been observed in the Malawi Rift and Thailand (Ring 1994; Morley 2010).

Nevertheless, uncertainty remains about the effects of these pervasive pre-existing structures and their influence on the propagation and linkage of fault segments during the evolution of a fault. In particular, questions remain about how the orientation and location of pervasive Precambrian gneissic foliations and regional joints influence the orientation of new normal faults and the location or geometry of linkage zones in rift systems.

Answering the question of how faults grow and evolve is important with implications for many fields in geology. Trudgill & Cartwright (1994) proposed a fault growth model where independent fault segments grow by linking with a progression from soft linkage (ductile deformation connecting fault segments) to hard linkage (brittle deformation connecting fault segments). In contrast, another fault growth model predicts the fast establishment of fault length before significant displacement (Walsh et al., 2003). Paton (2006) documented pervasive inherited structures perpendicular to extension that localized strain such that the faults followed the Walsh et al. (2003) type growth. Additionally, linkage geometry, due to the sensitivity of fault

tips to the local stress field, has also been suggested to be influenced by pervasive inherited structures (Trudgill & Cartwright 1994; Kinabo et al., 2008; Fossen & Rotevatn, 2016). Other work using modeling of Coulomb stress and fault linkage have shown that the existence of preexisting structures exerts an important control on the geometry of fault linkage (Hodge et al., 2018). Still, not much is known about these relationships for natural faults and how the pervasive inherited structures can affect the propagation of faults, impacting the nature of fault growth and evolution, which has a direct relationship to the potential for large magnitude earthquakes.

This study addresses the role of multiple pervasive inherited structures in influencing both the segmentation and the linkage of two >100 km long faults in the Malawi Rift: The Chirobwe-Ncheu and Bilila-Mtakataka faults. We document the gneissic Precambrian basement fabric and regional joints within the fault area using a combination of Shuttle RADAR Topography Mission (SRTM) Digital Elevation Model (DEM) data and for the first time in this region, high-resolution aeromagnetic data. These data allowed us to image the upper crustal structure of the basement fabric. In addition, we collected mesoscale structural data to verify the structural interpretations derived from remote sensing. This work proposes a new model for fault growth influenced by inherited fabrics which resulted in the formation of these >100 km long faults in the Malawi Rift.

.

CHAPTER II

TECTONIC SETTING

The Malawi Rift

The Malawi Rift represents the southern portion of the Western Branch of the East African Rift System (EARS; Figure 1; Chorowicz & Sorlien, 1992; Ring, 1994; Laó-Dávila et al., 2015). The Malawi Rift extends from Tanzania's Rungwe Volcanics to Mozambique's Urema Graben and is composed of northern, central, and southern rift segments (Ebinger et al., 1987; Laó-Dávila et al., 2015). The Malawi Basement Complex is Precambrian to lower Paleozoic in age and dominantly composed of paragneisses and granulites (Warshaw 1965; Dawson & Kilpatrick 1968; Thatcher 1969; Walter 1972). The age of the Malawi Rift is poorly constrained with dates ranging from 30 to 8 Ma from fission track dating and radiometric dating of volcanics, respectively (Ebinger et al., 1993; Van der Beek et al., 1998). The last major magmatic event occurred during the Cretaceous predating the onset of rifting (Ring, 1994). Currently, volcanic activity is constrained only to the Rungwe province which is at the northern extent of the Malawi Rift (Specht & Rosendahl, 1989). The Malawi Rift is broadly segmented into the Northern, Central, and Southern sections controlled by the lithospheric heterogeneities (Laó-Dávila et al., 2015). The Northern section is further segmented by half grabens which reverse polarity at approximately 100 km intervals (Daly et al., 1989; Specht & Rosendahl, 1989; Laó-Dávila et al.,

2015). The Central and Southern sections are defined by grabens, with less extension. In the Malawi Rift, the border faults are responsible for accommodating most of the extension (Ebinger et al., 1999). The modern rift has a regional E-W extension as seen from GPS data; however, focal mechanisms and kinematics suggest a local ENE-WSW extension with a rate of 1.5–2.2 mm per year (Figure 2; Delvaux & Barth, 2010; Fagereng, 2013; Saria et al., 2014; Stamps et al., 2018).

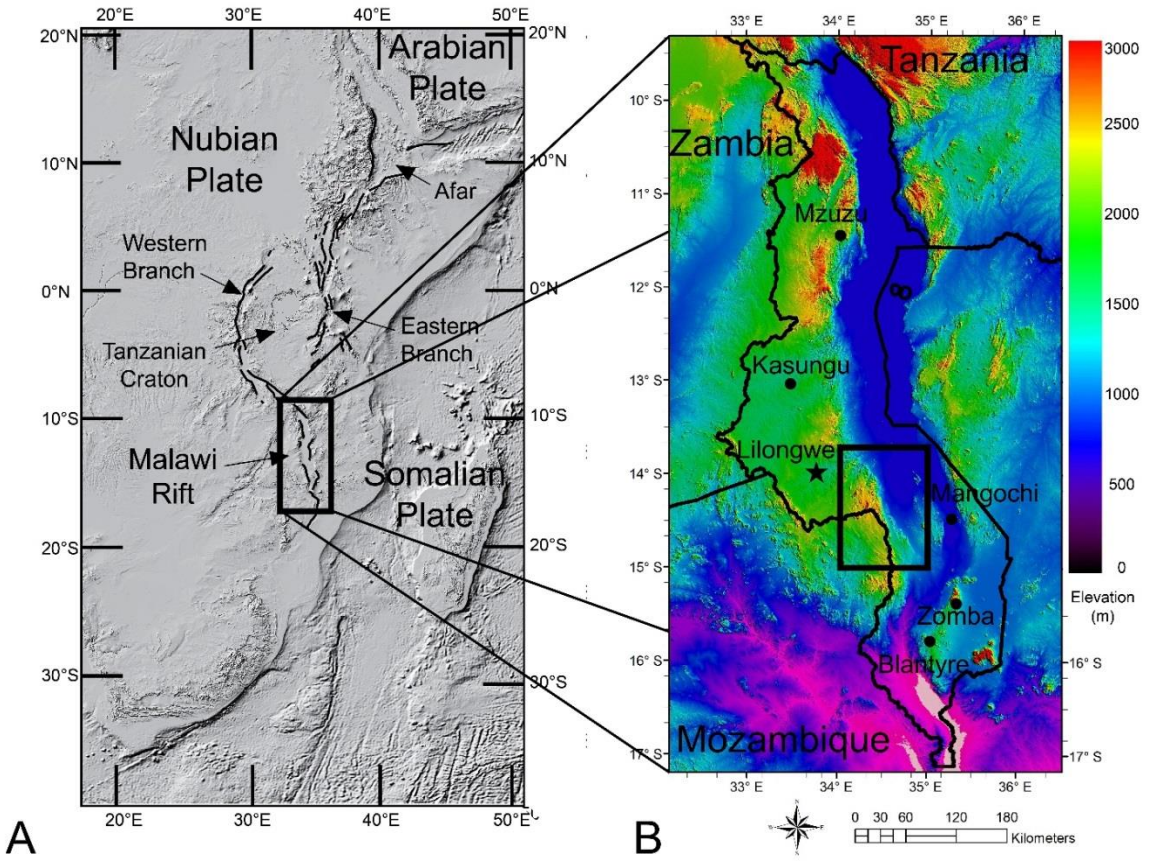

Figure 1: A) Tectonic map of the East African Rift System. B) Shuttle Radar Topography mission map showing a Digital Elevation Model of the Malawi Rift, country boundaries, and major towns. The black rectangle is the study area.

In Malawi some studies suggest that the Post-Proterozoic tectonic events caused regions of weakness which are affecting the modern rifting process (Piper, 1989; Versfelt & Rosendahl,

1989; Ring, 1994; Mortimer et al., 2016). Lithospheric scale inherited heterogeneities, such as Precambrian terrains and shear zones, are responsible for rift scale segmentation (Laó-Dávila et al., 2015; Mortimer et al., 2016; Kolawole et al., 2018).

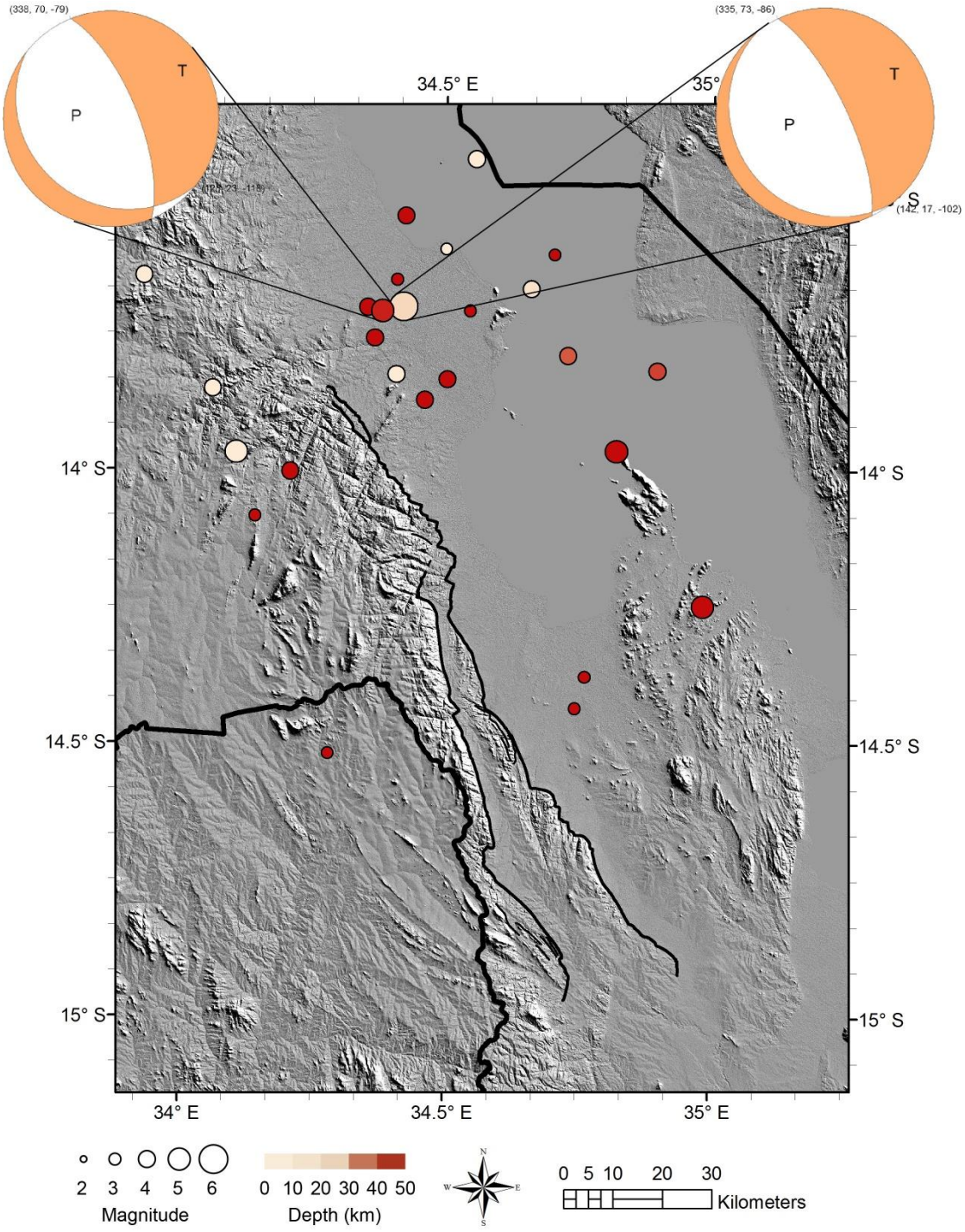

Figure 2: Earthquake epicenters near the study area as recorded by the earthquake catalog of the National Earthquake Information Center (NEIC). The two focal mechanisms where produced by the USGS Earthquake Hazards Program for the 6.2 Mb Salima seismic event of March 1989. The focal mechanisms support the NNE-SSW extension in this area.

The Chirobwe-Ncheu and Bilila-Mtakataka Fault Area

Our study area lies in the Central and Southern sections of the Malawi Rift (Figure 1; Laó-Dávila et al., 2015). The geology of the area is composed of Precambrian paragneisses characteristic of the Malawi basement complex and charnockitic granulites (Figure 3; Walshaw 1965; Dawson & Kilpatrick 1968; Thatcher 1969; Walter 1972). The gneissic foliations have a NNW strike in the south that changes to a NE strike in the north (Walshaw 1965; Dawson & Kilpatrick 1968; Walter 1972). From north to south, there is a WNW regional jointing pattern (Walshaw 1965; Walter 1972). The Cretaceous to upper Jurassic aged felsic dikes and quartz veins cut the Precambrian rocks (Walshaw 1965; Thatcher 1969; Walter 1972).

The study area is dominated by two east-dipping normal faults that follow the same general orientation as the preexisting gneissic fabrics (Walshaw 1965; Dawson & Kilpatrick 1968; Thatcher 1969; Walter 1972; Figure 3; Figure 4). The two faults are the outer and western Chirobwe-Ncheu Fault and inner Bilila-Mtakataka Fault (Jackson & Blenkinsop, 1997). The Chirobwe-Ncheu Fault is approximately 96 km long, has a NW strike, and scarp height of 300-1000 m (Jackson & Blenkinsop, 1997). Jackson and Blenkinsop (1997) suggests that the Chirobwe-Ncheu may be composed of three segments. In the southern and central areas, the Chirobwe-Ncheu Fault strikes parallel to the NW striking gneissic foliations except in the north where the fault turns to follow a NE striking foliation (Walshaw 1965; Dawson & Kilpatrick 1968; Thatcher 1969).

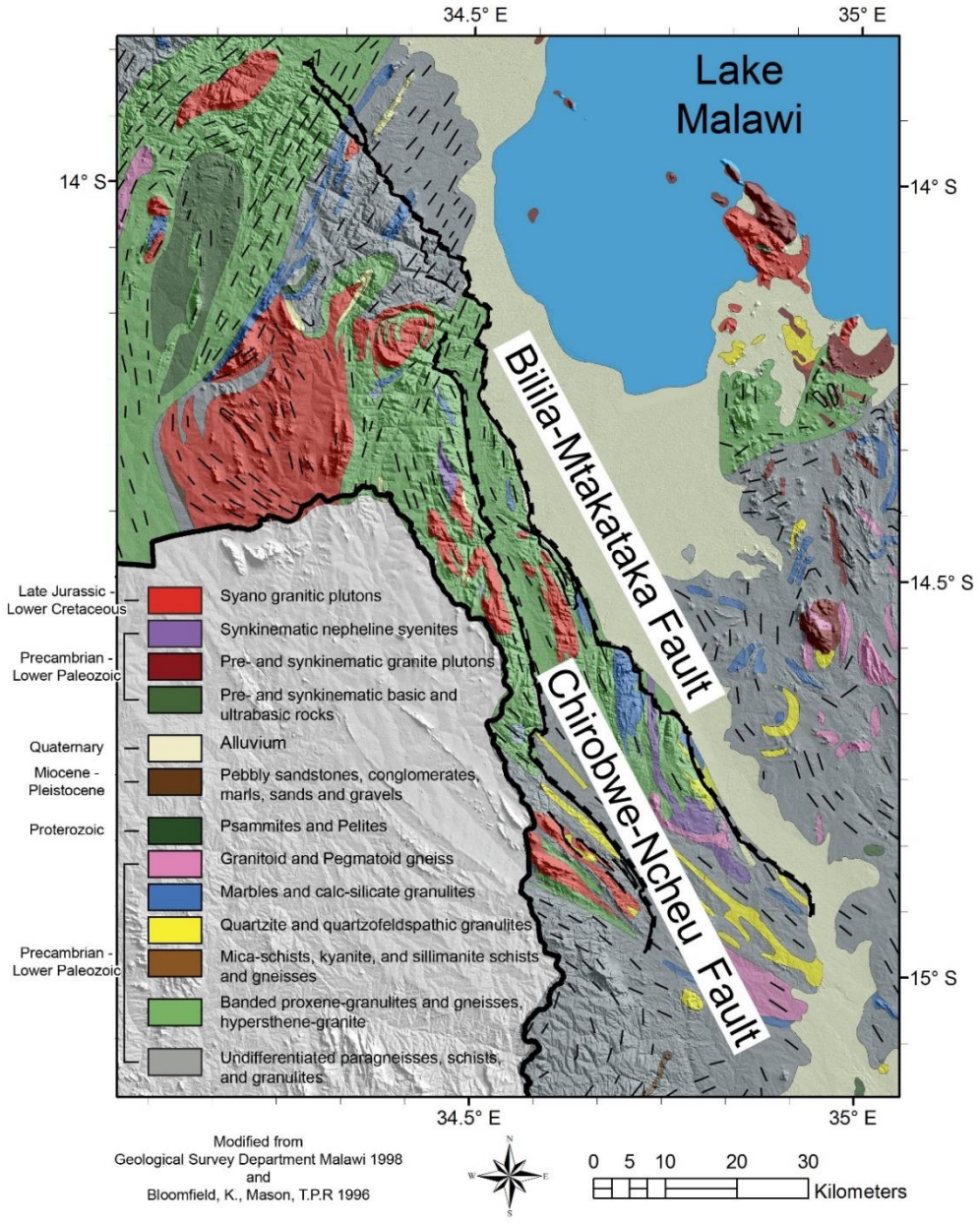

Figure 3: Geologic map of the study area overlaying an SRTM DEM (modified from Bloomfield & Mason, 1996). Structural information is from the Geologic Survey Department of Malawi (1998).

The Bilila-Mtakataka Fault is at least 100 kilometers long, with a 4.5-434 m high fault scarp, and a potential depth of 30 km due to deep seismicity and low heat flow in this area (Walshaw 1965; Thatcher 1969; Jackson & Blenkinsop, 1997; Ebinger et al., 1999; Fagereng,

2013; Njinju, 2016). In the southern part, the Bilila-Mtakataka Fault follows the gneissic foliations striking NNW until it turns to follow the joints with a WNW strike after which the fault continues to follow the foliations in the central region of the study area (Walshaw 1965; Dawson & Kilpatrick 1968; Thatcher 1969). The northern terminus of the Bilila-Mtakataka remains poorly constrained (Dawson & Kilpatrick 1968; Thatcher 1969; Jackson & Blenkinsop, 1997).

Figure 4: Photo looking to the south along the east dipping Chirobwe-Ncheu Fault scarp. To the left is the smaller Bilila-Mtakataka Fault scarp.

Lithospheric Structure in the Fault Area

Njinju (2016) used radially averaged 2D power spectrum of satellite gravity data to suggest the existence of a Niassa Craton due to thicker crust and asthenosphere depths to the west of our study area. Magnetotelluric and high-resolution aeromagnetic data suggest that for the same area the lithosphere of the Southern Irumide Belt is ~250 km deep, supporting the existence of a Niassa Craton (Sarafian et al., 2018). The deep seismicity (~40 km) reported by Yang & Chen (2010), Craig et al., (2011) and Fagereng, (2013) suggest a deep brittle crust which may be evidence for the existence of a Niassa Craton. If the Niassa Craton exists, then both the Chirobwe-Ncheu and Bilila-Mtakataka faults may be located at the edge of the craton. Thus, the formation of the faults may be the result of strain localization along the edge of the craton.

Seismic Hazard

Earthquakes in Malawi happen predominantly along the border faults of the rift, however there is also seismicity happening in the hanging wall (Chapola & Kaphwiyo, 1992; Biggs et al., 2010; Kolawole et al., 2018). Most seismicity is 10-20 km deep, however, seismicity 30-40 km deep has been recorded in southern Malawi (Biggs et al., 2010; Yang & Chen 2010; Craig et al., 2011; Fagereng, 2013). The maximum depth for seismicity is 44 km ± 4 (Yang & Chen 2010; Craig et al., 2011; Fagereng, 2013). It is well understood that the geometry of a fault governs the seismic potential; therefore, the >100 km large Chirobwe-Ncheu and Bilila-Mtakataka faults have a potential to produce large magnitude earthquakes (Jackson & Blenkinsop, 1997; Craig et al., 2011; Fagereng, 2013; Hodge et al., 2015). The Bilila-Mtakataka in particular has been suggested to potentially yield a magnitude 8.0 earthquake (Jackson & Blenkinsop, 1997; Craig et al., 2011; Fagereng, 2013; Hodge et al., 2015). The seismicity for the study area recorded by the USGS has been plotted in Figure 2.

CHAPTER III

METHODOLOGY

Shuttle Radar Topography Mission Data and Processing

In our study we used Shuttle RADAR Topography Mission (SRTM) one-arc-second data from NASA which has spatial resolution of 30 m and a vertical accuracy of approximately 5 m for Africa (Mukul et al., 2015; Rodriguez et al., 2006). The SRTM data was processed in Environment for Visualizing Images (ENVI) software to generate hill-shaded Digital Elevation Models (DEM) used to delineate the faults and topographically expressed basement lineaments. Arc GIS's Arc Map was used to extract topographic profiles offset at a constant 1 km interval and oriented perpendicular to each fault. Those profiles were used to determine the fault throw at the 1 km sampling interval with the assumption that the topography was the result of rifting. We then assumed fault dips of 60° as predicted by Andersonian type normal faulting to calculate the minimum apparent displacement following the methods of Muirhead et al. (2016). These minimum apparent displacement plots are subsequently referred to as simply displacement profiles. We used the displacement profiles to establish the segmentation of the Chirobwe-Ncheu and Bilila-Mtakataka faults. Segmentation is defined as kinematically distinct portions of a larger fault represented by smaller independent faults with distinct displacement trends (Trudgill & Cartwright, 1994; Walsh et al., 2003). The profiles were qualitatively smoothed by removing high

frequency low displacements to better reflect a surface less affected by weathering. Then we looked for peaks in displacement bound on both sides by low displacement similar to the ideal displacement profile for a fault (Figure 5). Using this method, we established a first order segmentation for each fault. Once the length of the faults had been established, both the fault strikes and SRTM DEM derived lineament orientations where extracted with Arc GIS. The orientations were plotted in rose diagrams using the Stereonet 9 program (Allmendinger et al., 2012; Cardozo and Allmendinger, 2013).

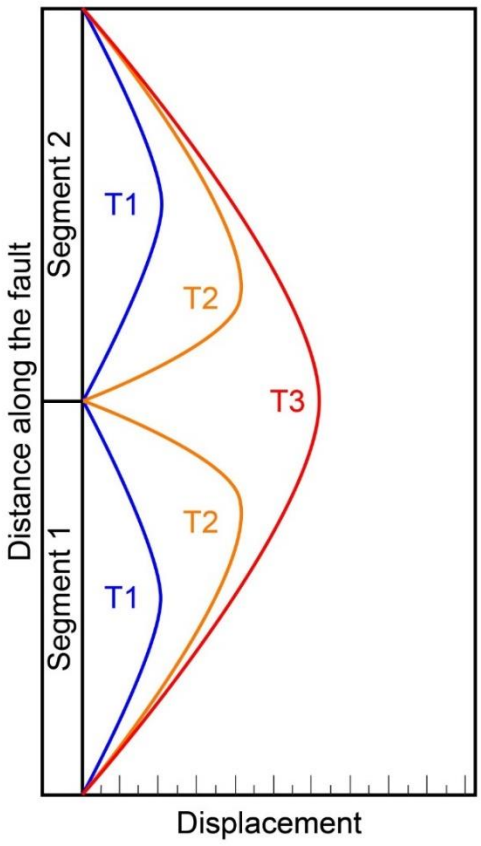

Figure 5: An idealized displacement model showing the evolution through time of linkage between two segments (Kim & Sanderson, 2005). T1 is the earliest stage with both segments having distinct and independent displacement profiles with no linkage. T2 is the soft linkage between the two segments as they begin to link to one another yielding asymmetric profiles. T3 is the final stage showing the two segments hard linked together with a single displacement profile for both original segments.

Aeromagnetic Data and Processing

The high resolution aeromagnetic data of Malawi was collected by the Malawi Ministry of Mining in 2013. The flight lines had an orientation of NE-SW with a line spacing of 250 m and

control lines were oriented NW-SE with a line spacing of 5000 m. The flight was conducted using a draped flight height of 60 m.

A grid cell size of 50 m was used in our study. The aeromagnetic data was first reduced to pole. The process of reduction to pole transforms the magnetic data so that it acts as a vertical vector and corrects the spatial location of magnetic anomalies (Baranov 1957). We then applied derivative filters to accentuate the magnetic features. The tilt derivative, which is the vertical derivative divided by the total horizontal derivative of the magnetic field (Miller & Singh, 1994), was calculated to delineate the magnetic fabric as shown by Oruç & Selim (2011). Arc GIS was then used to extract the orientation of the lineaments derived from the tilt derivative using the identical method used for the SRTM lineaments.

Source Parameter Imaging (SPI) is a method for estimating depth using a depth model derived from the wavenumber of the analytic signal (Thurston & Smith, 1997). SPI gives the depth to the magnetic source; however, SPI is known to be sensitive to noise (Thurston & Smith, 1997). SPI has been reported to have an accuracy of ±20% by Oasis Montaj. SPI acts as a proxy for segmentation because along a normal fault the expected depth will be deeper for the hanging wall than the footwall and the variations in depth of the hanging wall will reflect the general segmentation of the fault. The spatial distribution rather than the absolute magnitude of the SPI predicted depth can be used as a proxy for displacement to support the segmentation of the displacement profiles derived from SRTM DEM.

Mesoscale Structural Data

Structural information was collected from foliations, dikes, and joints at various outcrops along roads and streams to verify the orientations observed with remote sensing. The data was grouped based on the type of structure to facilitate an understanding of which structures are

affecting the faults (Figure 6). The data was collected in July of 2017 using a Brunton Compass and plotted as stereographic projections using Stereonet 9.

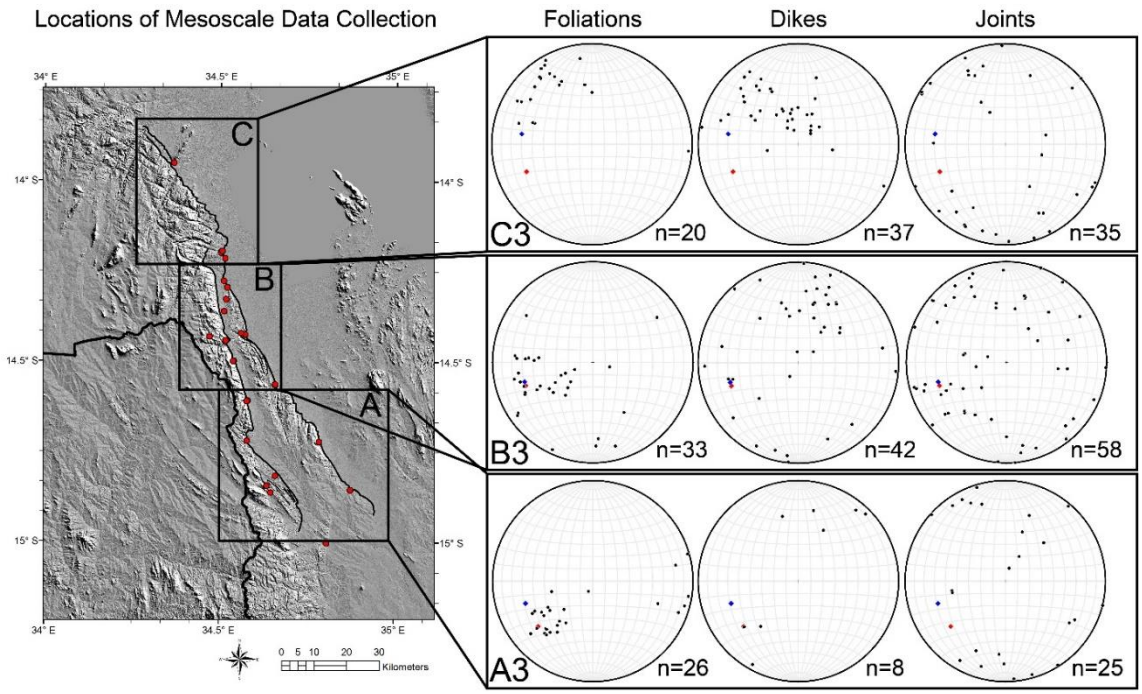

Figure 6: SRTM DEM of the study area showing regions and sites where mesoscale data were collected (red circles). Stereographic projections show poles to foliations, dikes, and joints for each region. The average strike for both Chirobwe-Ncheu (blue diamond) and Bilila-Mtakataka (red diamond) faults is shown with an assumed ideal Andersonian 60° dip to the east.

CHAPTER IV

RESULTS

Displacement Profiles, Segmentation, and Linkage of the Border Faults

Our first step was to characterize the segmentation of each fault. The displacement profiles Figure 7 shows that the Chirobwe-Ncheu Fault has a length of 102 km as measured along the length of the fault scarp. The average displacement is 430 m with a minimum of 12 m and a maximum of 1137 m. The Chirobwe-Ncheu Fault can be broken into three segments CN1, CN2, and CN3. The segments CN2 and CN3 are characterized by high displacement (>700 m). In contrast, the southern segment CN1 has low displacement (<400 m). Segment CN1 is connected to the north to CN2 by linkage zone CN1-2 with a displacement of ~75 m. Segments CN2 and CN3 are connected by a linage zone CN2-3 with ~385 m displacement. Segment CN2 has an asymmetric displacement profile which is skewed to the north. Segment CN1 has a D shaped profile and CN3 has a well formed D shaped displacement profile typical of an ideal independent fault segment.

The Bilila-Mtakataka Fault has a length of 159 km measured along the fault scarp length. This fault has an average displacement of 187 m, a minimum of 16 m, and a maximum of 627 m. The fault can be divided into three segments (Figure 7) based on the ideal form of a displacement profile (Figure 5). Linkage BM1-2 is a relative low between two peaks with ~140 m of

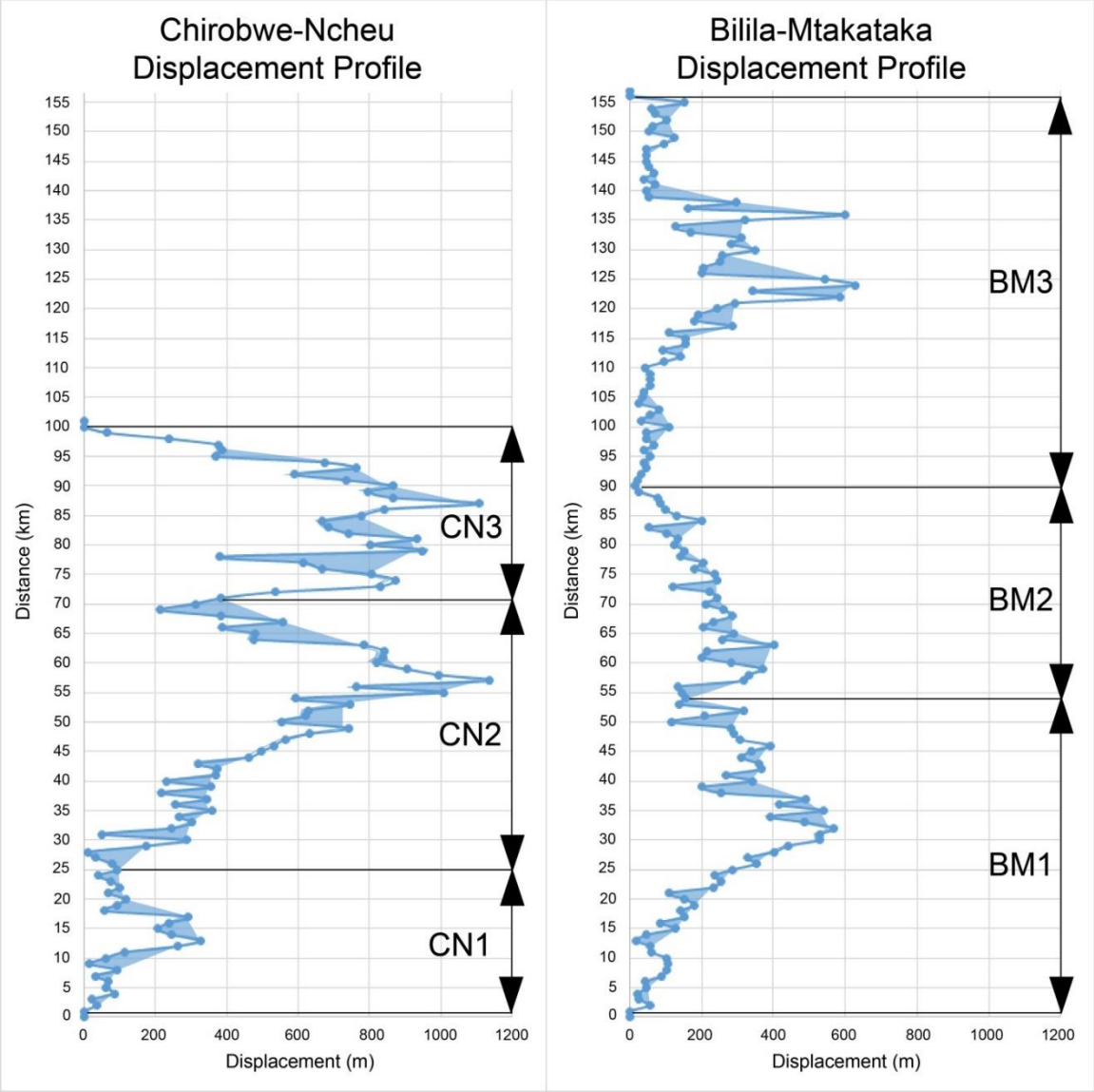

Figure 7: Displacement profiles and segmentation for both the Chirobwe-Ncheu and Bilila-Mtakataka faults calculated from SRTM DEM topographic profiles. The profiles where collected at 1 km offset and perpendicular to the fault scarp. The blue areas represent a proposed eroded surface. The segments are named according to fault and numbered from south to north.

displacement. Linkage BM2-3 has the lowest displacement of ~25 m. The southernmost segment BM1 is skewed slightly to the north. The segment BM2 is asymmetrically skewed to the south. BM3 has a well formed D shaped symmetrical displacement profile with maximum displacement in the center and decreasing displacement towards the segment tips.

The displacement profiles were used to constrain the end points of the faults (Figure 8; Figure 9). The lateral variation in strike for each of the faults was plotted in rose diagrams (Figure 10). For our study area, we divided it into three regions: the southern Region A, the central Region B, and the northern Region C. In Region A, the Chirobwe-Ncheu and Bilila-Mtakataka faults have diffuse distribution of fault strikes with a general NW strike. In Region B, both the Chirobwe-Ncheu and Bilila-Mtakataka faults have a consistent NW strike. In Region C, the Chirobwe-Ncheu Fault has a wide distribution with an overall NE strike. The Bilila-Mtakataka Fault however, has a wide distribution of strikes ranging from NW to N.

The surface expression of the inherited structures were traced as lineaments from the SRTM DEM data in red and plotted in rose diagrams (Figure 9; Figure 10). In Region A, the lineaments had four dominant orientations: WNW, NW, N-S, and NNE. In Region B, the lineaments had a prevailing E-W strike with two other minor strikes to the NW and NNE. In Region C, the rose diagram shows lineaments striking to the WNW and to the NE. The lineaments represented as peaks in the rose diagrams were interpreted as either joints or foliations.

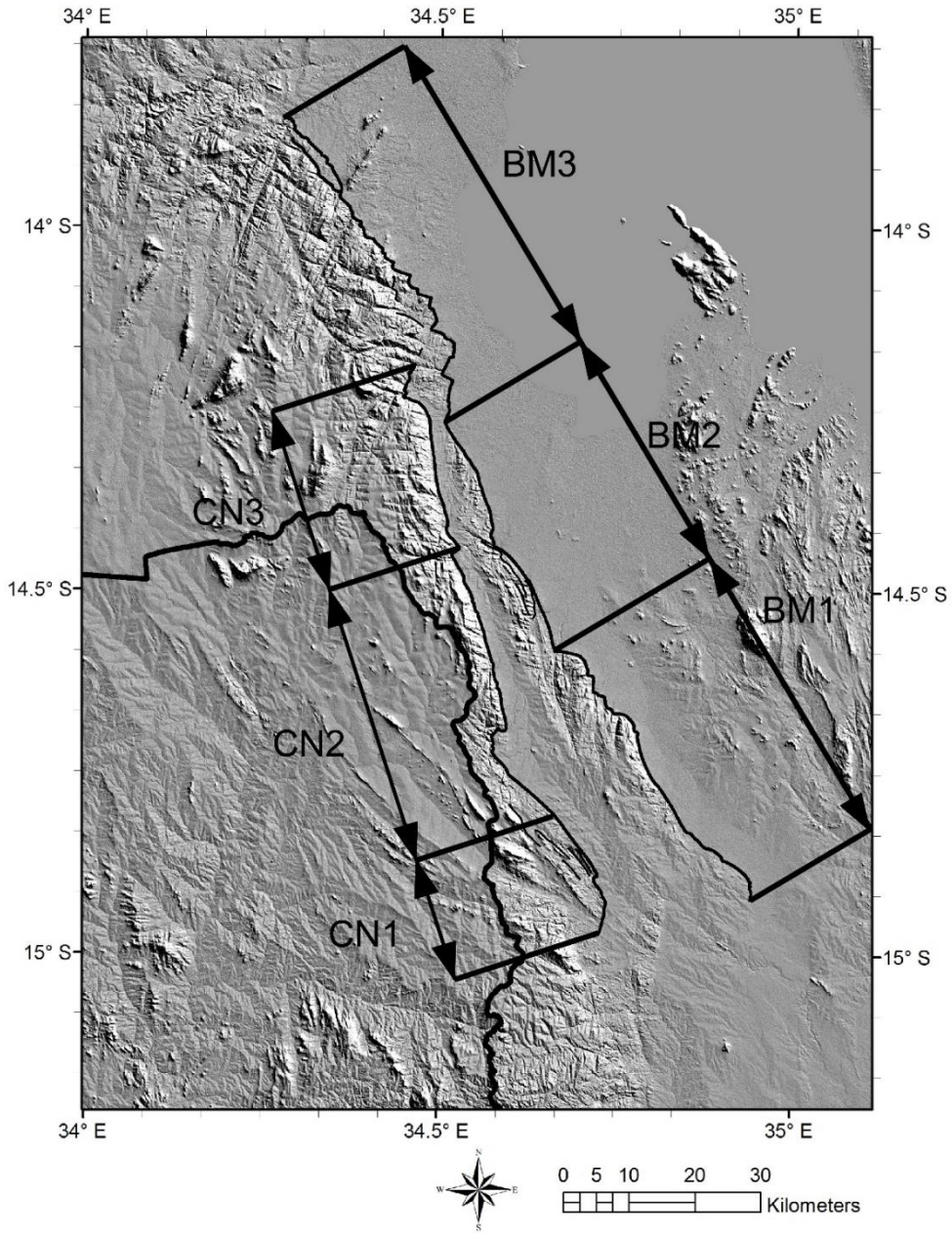

Figure 8: The segmentation from the displacement profiles represented in map view overlaying the SRTM DEM.

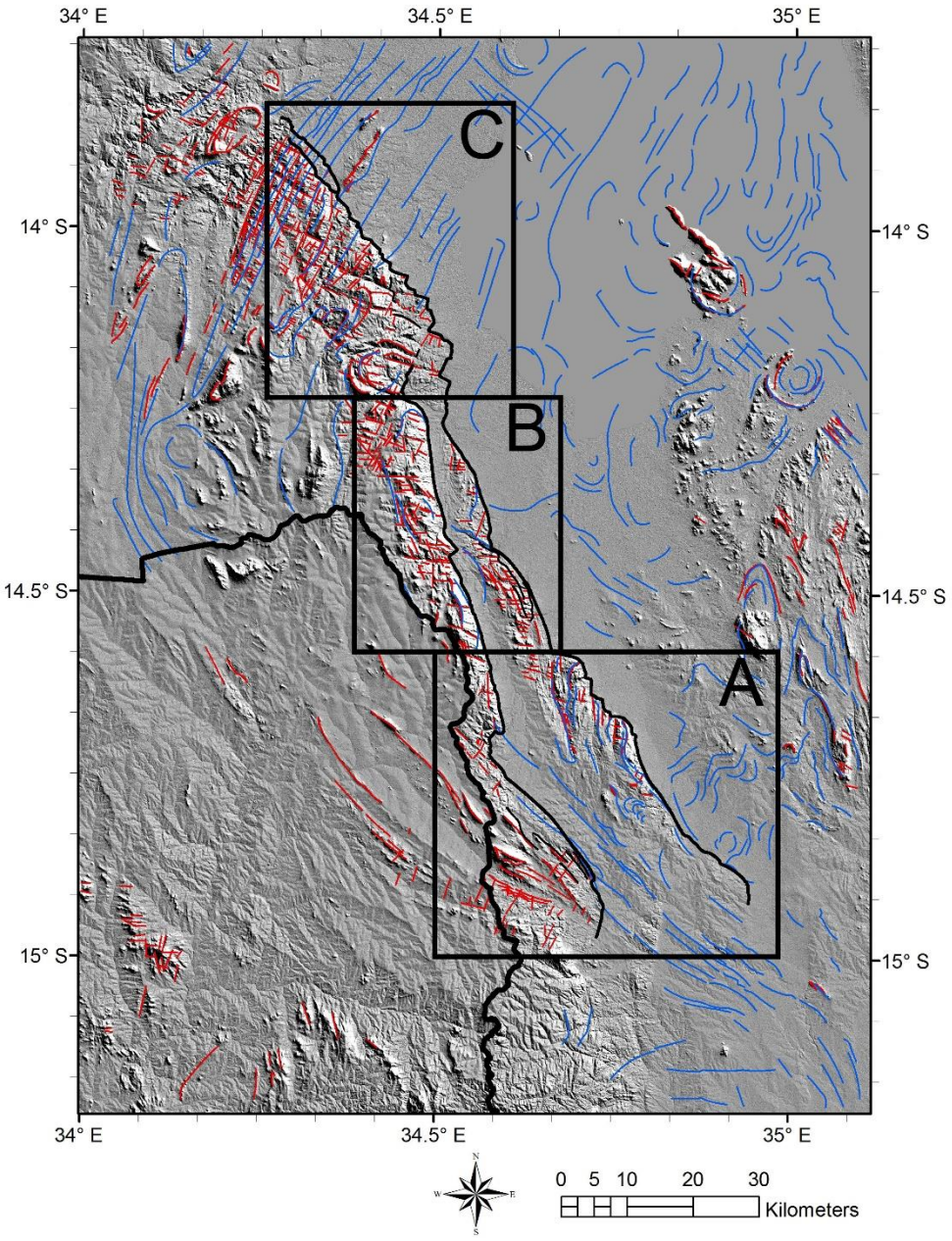

Figure 9: Lineament map of the study area. Red lineaments were mapped from the SRTM DEM. Blue lineaments were mapped from aeromagnetic data.

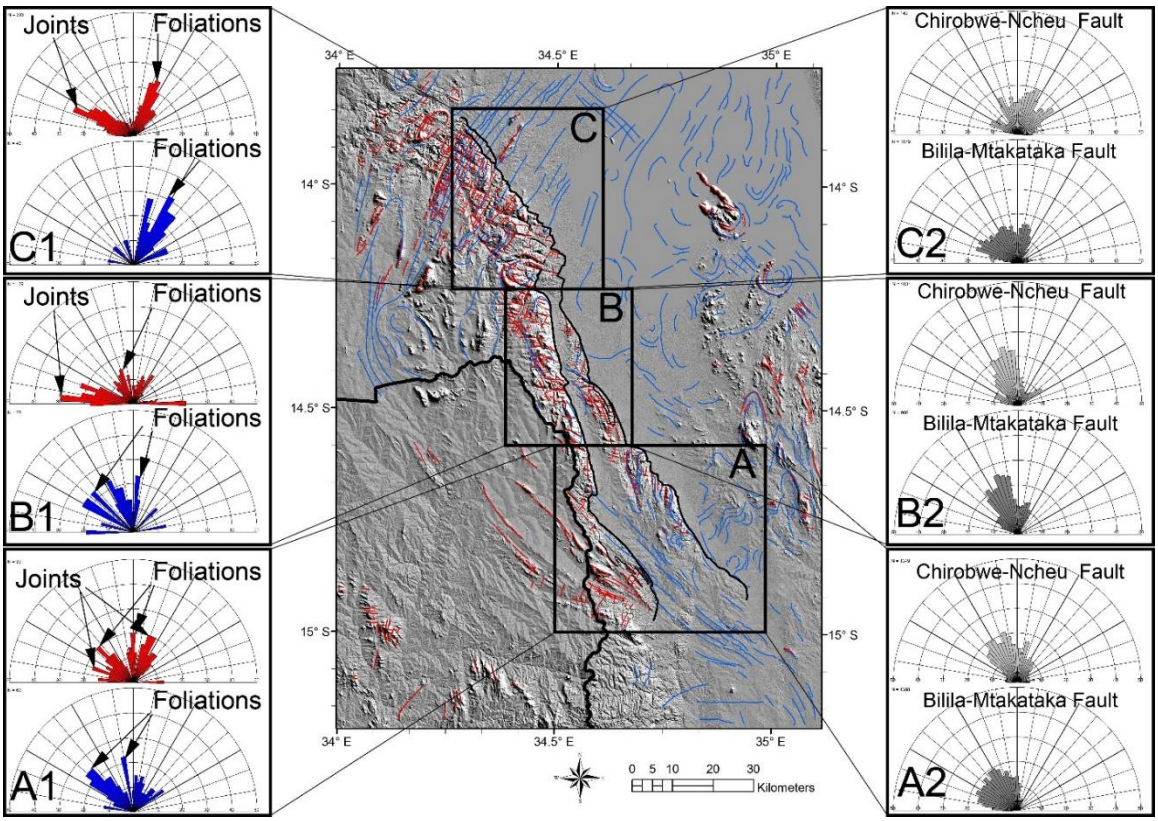

Figure 10: Lineament map of the study area. Red lineaments were mapped from the SRTM DEM. Blue lineaments were mapped from aeromagnetic data. A1, B1, and C1 are rose diagrams for trends of lineaments interpreted as foliations and joints. A2, B2, and C2 are rose diagrams for strike of each fault. The strike of the faults was taken from breaking the SRTM DEM fault traces at the line vertexes and computing the orientation for each of these segments.

Aeromagnetic Results

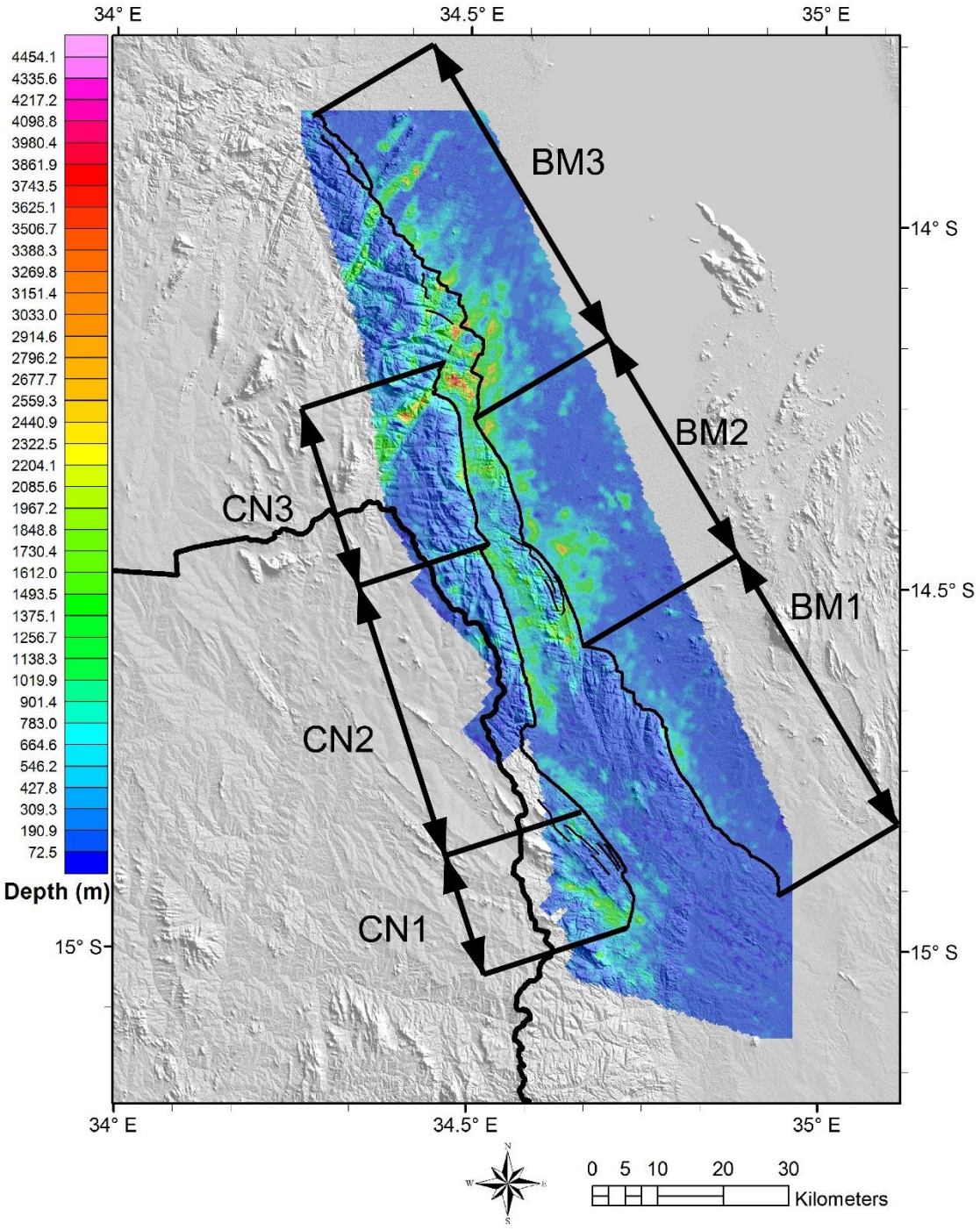

Figure 11: A map of SPI overlain by a SRTM DEM. The blue represents a shallow depth to magnetic source. The green corresponds to a larger depth to magnetic source and red is the greatest depth to magnetic source. Segmentation derived from the displacement profiles are shown to better facilitate comparison between the two data sets.

The SPI predicted depths for the area are shown in Figure 11. In general, the SPI map shows deeper anomalies to the east of the Chirobwe-Ncheu and Bilila-Mtakataka faults. In the south, the Chirobwe-Ncheu Fault has diffuse depth anomalies with a NW trend. The central and northern areas of the fault (CN2 and CN3) has clearly defined deep anomalies separated by a relative high between them. This relative high (shallower depth to magnetic basement) corresponds well to the linkage regions CN2-3 and BM1-2 mapped from the SRTM DEM displacements. At the northern end of the Chirobwe-Ncheu Fault there is a broad deep (~4000 m) magnetic depth anomaly. The southern portion of the Bilila-Mtakataka Fault has shallow depths in the SPI map. The central region of the fault is characterized by an anomaly that is spatially larger in the south and decreasing to the north. This trend of deeper depths in the south which decreases northward is also reflected in segment BM2 in the displacement profiles. In the northern region the SPI depths have deep anomalies with NE trends.

The tilt derivative of the aeromagnetic data (Figure 12) was used to map the subsurface basement structures like the gneissic fabrics of the Malawi basement complex, which are not well expressed in the SRTM DEM. The tilt derivative delineated folds, gneissic fabrics, and a circular granite body. The magnetic lineaments mapped from the tilt derivative map is shown as blue in Figures 9 and 10. The rose diagrams represent the trends of the magnetic lineaments. In Region A, the magnetic lineaments have two orientations NW and NNW. In Region B, the lineaments have a noncontiguous NW strike. In Region C, the magnetic lineaments have a NE strike. The general trend of the magnetic lineaments changes from NW in Region A to NE in the Region C

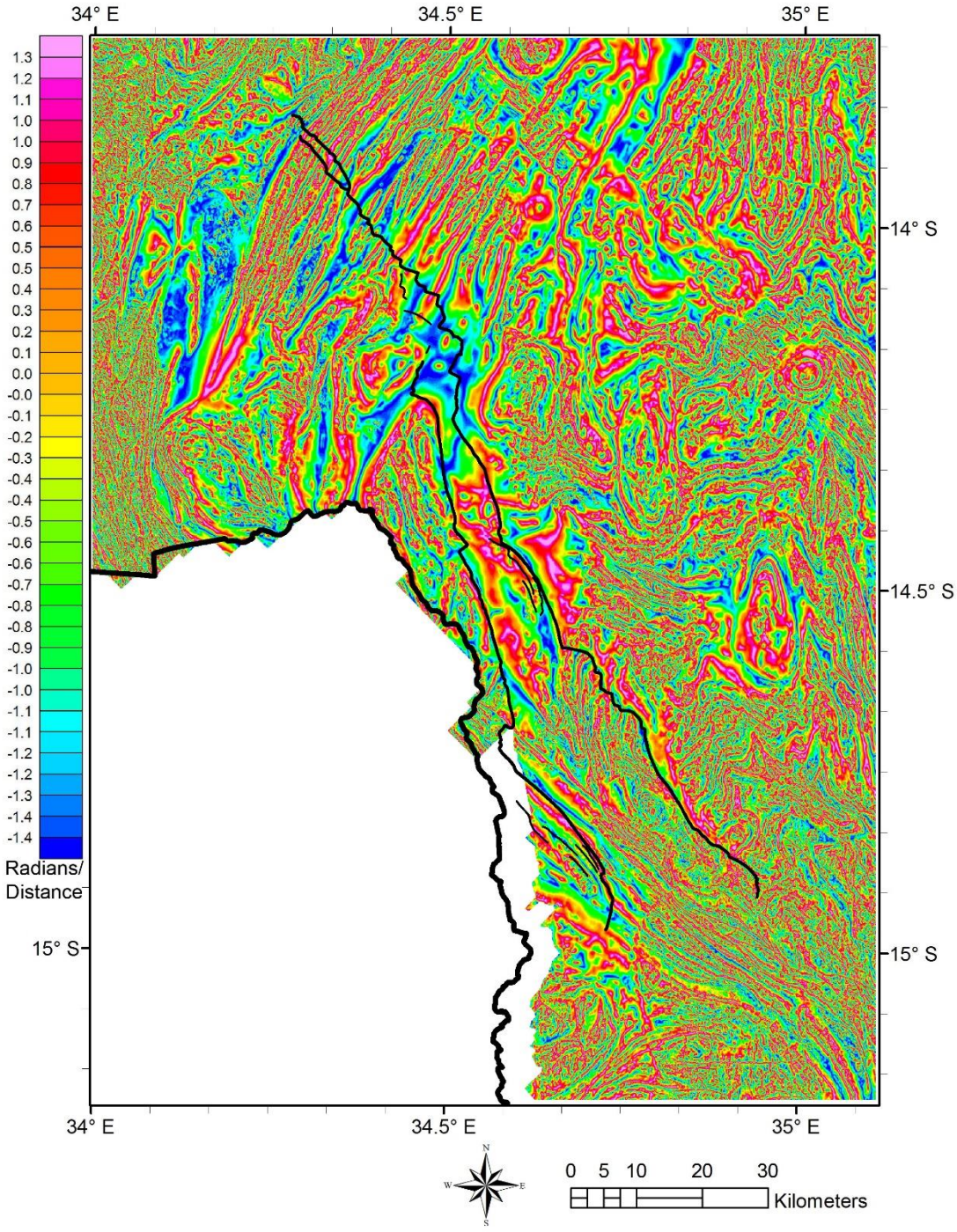

Figure 12: Aeromagnetic tilt derivative map for the study area. The negative colors (Green, Cyan, and Blue) are west dipping and the positive colors (Orange, Red, and Pink) are east dipping. Yellow represents the zero contours.

Mesoscale Structures

Mesoscale structures were documented throughout the study area (Figure 13). The orientations of mesoscale structures are shown in Figure 6 with the average strikes for both Chirobwe-Ncheu and Bilila-Mtakataka faults for each region. The foliations have a NNW strike and NE dip in Region A, N-S strike and E dip in Region B, and a NE strike with a SE dip in Region C. The dikes have a NW strike in Region A, E-W strike and S dip in Region B, and a NE strike and SE sip in Region C. The joints have no clear dominant orientation in this data set. The mesoscale structures reveal in Region A that the strike of the foliations and the faults are similar. The strike of the dikes and joints has a general E-W orientation and no relationship to the fault's dominant strike. Within Region B, the foliations and the faults continue to have a similar strike. In Region C, the foliations and strike of the Chirobwe-Ncheu Fault have a similar orientation, however, the strike of the Bilila-Mtakataka Fault is to the NW.

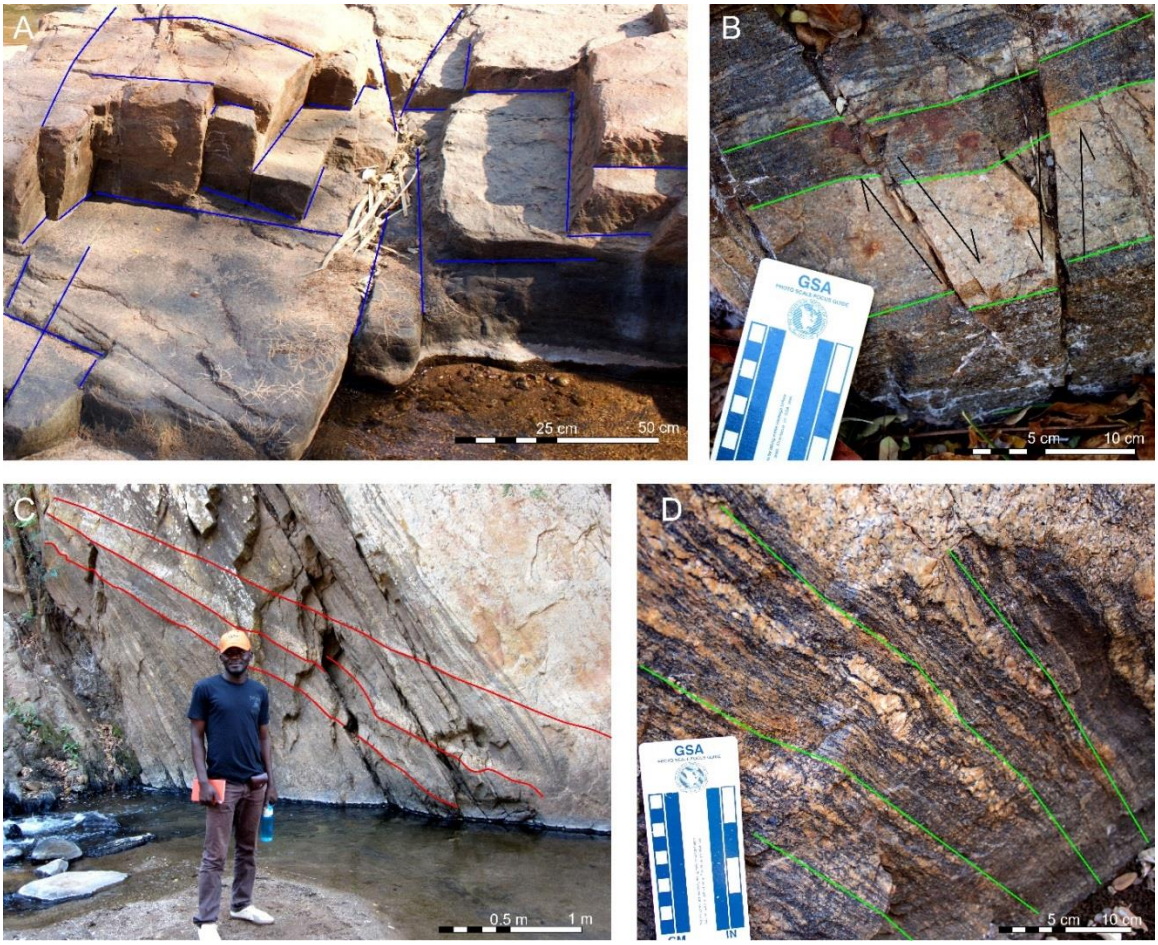

Figure 13: Photographs of mesoscale structures in the study area. A) Orthogonal joints. B) Conjugate normal faults. C) Felsic dikes. D) Gneissic foliations typical of the Malawi Basement complex.

CHAPTER V

DISCUSSION

Interpretation of Structural Lineaments

The orientation of the aeromagnetic lineaments corresponds with the orientation of gneissic foliations we mapped from outcrops (Figure 6) and those documented by Walshaw (1965), Dawson & Kilpatrick (1968), Thatcher (1969), Walter (1972), the Geologic Survey Department of Malawi (1998), and Hodge et al., (2018). The SRTM DEM reveals both topographically expressed gneissic fabric and jointing patterns. Some of the ridges in the SRTM DEM parallel the gneissic fabric of the area documented in the aeromagnetic data, mesoscale structures, and maps of the Geologic Survey Department of Malawi (1998). Additionally, the gneissic foliations have been shown to influence faulting and lead to the developing of stepping or en échelon fault segments (Kolawole et al., 2018; Muirhead & Kattenhorn 2018). The continued development of these segments would lead to the development of a fault system which follows closely the gneissic foliations we see in the study area. Additionally, the other SRTM DEM lineaments correspond to the jointing patterns documented by Walshaw (1965), Dawson & Kilpatrick (1968), Thatcher (1969), and Walter (1972). The lineaments that represent the jointing patterns were interpreted as such because they have no vertical displacement, have a spatially constant strike characteristic of joints which have developed in a single stress regime, and these

lineaments correspond to the joint sets described by Walshaw (1965), Dawson & Kilpatrick (1968), Thatcher (1969), and Walter (1972). The existence of the joints exhibiting the same orientation outside the study area and distally located to the Cenozoic rifting suggests that these fractures are preexisting to the modern rift and possibly related to the Karroo Rifting of late Paleozoic to early Mesozoic age.

The Chirobwe-Ncheu Fault

The southernmost segment of the Chirobwe-Ncheu Fault (CN1) is characterized by low displacement and a D shaped symmetrical displacement profile (Figure 7). The SPI does not show any significant displacement in this area (Figure 11). This small fault segment may represent an independent fault which has recently linked to CN2. In this area the mesoscale structure data, SRTM lineaments, and the aeromagnetic lineaments have the same strike of the fault segment suggesting that the orientation of this segment resulted from the gneissic foliation. The presence of a low displacement fault segment and the segment formation parallel to the gneissic fabrics are suggestive that CN1 is a Walsh et al. (2003) type fault segment which propagated along the gneissic foliations achieving a long length before experiencing significant displacement. The linkage of CN1 and CN2 is a soft linkage between a small distinct fault and the northern segments which have higher displacement and constitute the majority of the Chirobwe-Ncheu Fault.

The central segment CN2, has an SPI and displacement profile that suggest ~1000 m of displacement. CN2 has an asymmetric displacement profile which is skewed to the north. CN2 follows very closely the NNW oriented gneissic foliations mapped by the mesoscale structure data, SRTM lineaments, and the aeromagnetic lineaments which are well aligned for the ENE-WSW extension. The linkage of segments CN2 and CN3 are represented by a hard linkage with

low displacement, shallow SPI depth, and asymmetric displacement profiles. This linkage corresponds to a cross cutting magnetic lineament seen in the tilt derivative map, which possibly inhibited the fault development leading to the propagation of segments on either side (Figure 12). The linkage of CN2-3 is characteristic of Trudgill & Cartwright (1994) type fault linkage because both segments have large displacement and exhibit asymmetry towards the linkages zone.

The northern segment of the Chirobwe-Ncheu Fault (CN3) also has high displacement shown by both the displacement profiles and the SPI (Figure 7; Figure 11). CN3 follows the gneissic fabrics with a NNW strike mapped with the mesoscale structure data, SRTM lineaments, and the aeromagnetic lineaments. The fault follows the basement fabric so closely that it curves from a NW to an E-W strike following a fold in the gneissic basement (Figure 14E). This relationship suggests that the gneissic foliations localized strain leading to the development of a sub-parallel fault, which follows the gneissic foliations. In the north, the Chirobwe-Ncheu Fault interacts with a preexisting (Late Jurassic to Early Cretaceous) syeno-granitic pluton. The contact between the pluton and the gneiss localized the stress resulting in the fault to curve to the NE before terminating.

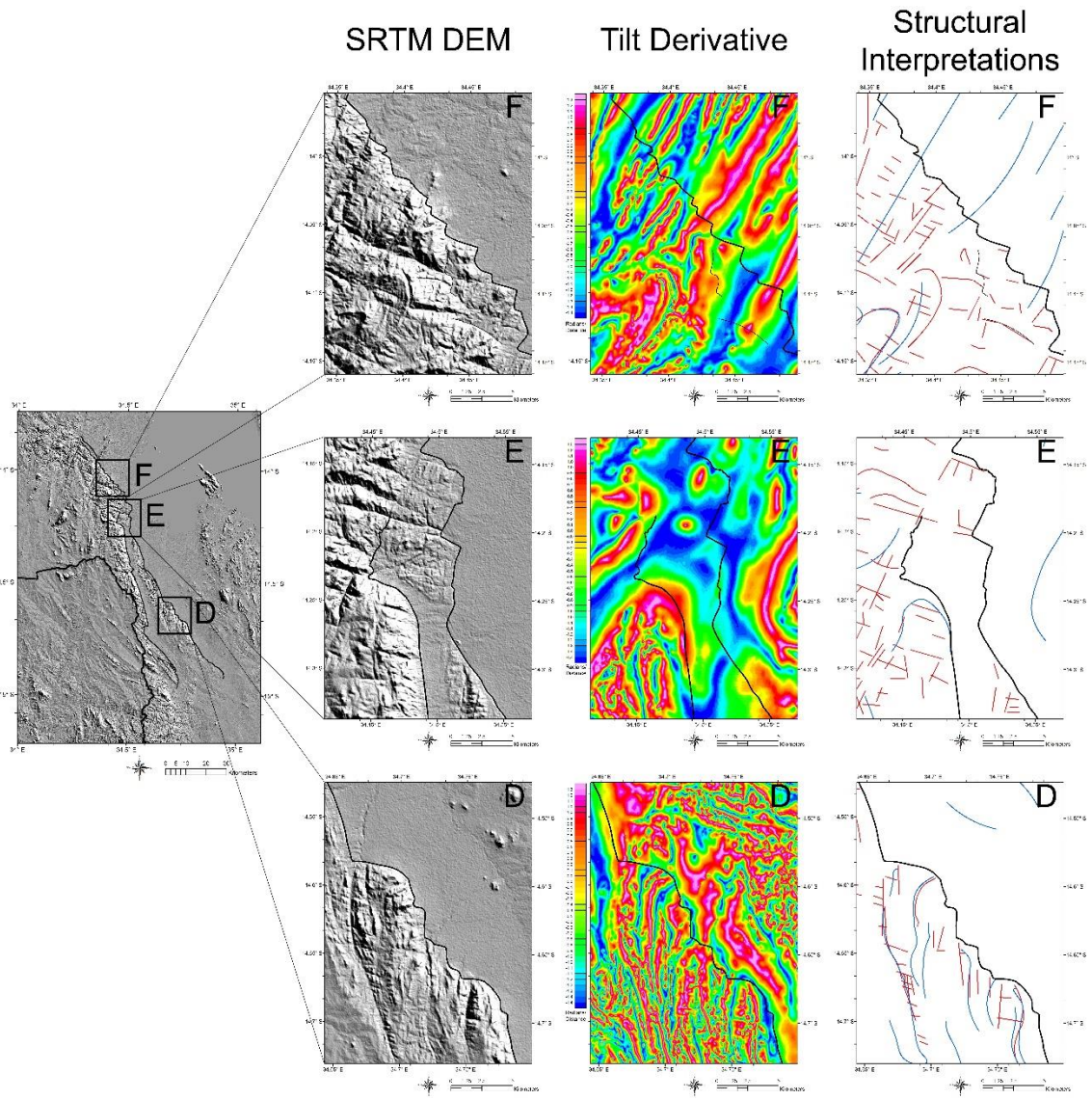

Figure 14: A closer look at regions shone on the left which highlight the role that inherited structures have played in influencing the development of the faults. The regions D, E, and F are shown on the left with an SRTM DEM and in the center as a tilt derivative. The column on the right is our structural interpretations of the regions where the red lineaments are derived from the SRTM DEM and the blue lineaments are from the tilt map.

The Bilila-Mtakataka Fault

The southernmost segment of the Bilila-Mtakataka Fault (BM1) is characterized by a segment with northward skewed displacement profile (Figure 7). The displacement is also

reflected in the SPI depths (Figure 11). In the south, the fault propagates parallel to the N-S striking gneissic fabric documented in the mesoscale structure data, SRTM lineaments, and the aeromagnetic lineaments. However, in the north the strike of BM1 crosscuts the magnetic lineaments instead zig-zagging between NNE and WSW strikes, which are subparallel to the gneissic foliations and regional joints, mapped by the mesoscale structure data and the SRTM lineaments. This suggests that the fault nucleated and propagated initially along the gneissic foliations. Figure 14D shows the linkage zone between segments BM1-2. The linkage is characterized by low displacement and shallow depths in the SPI. The asymmetry of BM1 and BM2 is suggestive that the segments are hard linked as expected in the Trudgill & Cartwright (1994) type fault linkage.

The central segment BM2 has an asymmetric displacement profile skewed to the south, which is also represented in the SPI (Figure 7; Figure 11). In this area, the mesoscale structure data, SRTM lineaments, and the aeromagnetic lineaments show the NW striking gneissic foliation and the fault. The fault segment has a curved trace very similar to the curves of the gneissic foliation (Figure 14E). This relationship supports the idea that the fault nucleated and propagated along the gneissic foliation, which is perpendicular to the ENE-WSW extension. The linkage BM2-3 is represented by a point of low displacement and a change in fault strike (Figures 7 and 14E).

The displacement profile for BM3 is D shaped; therefore, the linkage of BM2-3 is a soft linkage between two distinct fault segments. The long length of BM3 with low displacement tips suggests that this segment grew quickly as predicted in the Walsh et al., (2003) type growth. This rapid growth is likely facilitated by the pervasive preexisting structures allowing for rapid establishment of the segments length. The northern segment of the Bilila-Mtakataka Fault (BM3) has a symmetric displacement profile. The fault has a jagged morphology and large variability of strike (Figure 14F). This segment cuts at high angle the gneissic foliations mapped with the

SRTM and aeromagnetic lineaments. The fault has a jagged morphology with an average NW strike. In this area, the regional jointing pattern has a WNW strike and the gneissic foliations have a NE strike. This presence of two prolific fabrics results in a zig-zag fault geometry as the fault propagated along both the reginal joints and the gneissic foliations, similar to the northern portion of BM1 (Figure 14D). For this area the preexisting pervasive upper crustal fabric affects the orientation and geometry of BM3 causing the distinct morphology of this segment.

The Influence of Structural Inheritance in the Upper Crust

The orientation and location of Precambrian foliations, and regional joints suggest that both the segmentation and linkage of these two normal faults are controlled at least in part by the pervasive inherited structures. Our results show that the orientations of the Chirobwe-Ncheu and Bilila-Mtakataka faults resemble the orientations of the gneissic foliations and the regional joints. Faults in regions A and B show a close correlation with the gneissic foliations, suggesting that the faults are exploiting the gneissic foliations which localize the extension. Segments CN2, CN3, BM1, and BM2 show large displacement in both the displacement profiles and in the SPI depths representing well-developed fault segments. The strike of these segments also correlate to the strike of the gneissic foliations. Thus, for these segments, the faults nucleated and propagated along the foliations before linking. In contrast, the segments CN1 and BM3 show long faults with lower displacements when compared with the other segments. These segments where likely able to propagate due to the existence of pervasive upper crustal fabrics, similar to a Walsh el at. (2003) type fault growth. BM3 and the northern segment of BM1 show that a fault can make use of multiple structures (i.e. the reginal joints and gneissic foliations) as it propagates. The influence of pervasive oblique inherited structures yielding zig-zag fault geometry seen in BM3 and parts of BM1 has been documented in the analog models of Henza et al. (2011) and

Chattopadhyay & Chakra (2013). The existence of preexisting pervasive upper crustal fabrics has affected the orientation and geometry of both the Chirobwe-Ncheu and Bilila-Mtakataka faults.

The fault linkage is also affected by the pervasive upper crustal fabrics. In the linkage zone BM1-2, the fault segments are clearly propagating along the gneissic foliations and the linkage is then facilitated by the regional jointing pattern localizing the strain resulting from fault tip overlap. In this area, the N-S striking foliations are well oriented for activation by the rift faults while the less prolific E-W regional joint sets are well oriented to facilitate linkage between segments. Additionally, the linkage CN2-3 is the result of a cross cutting magnetic lineament, which may have prohibited the propagation of the segments and ultimately resulted in the formation of a linkage zone there. The linkage of BM2-3 is represented by the fault transitioning for propagation along the gneissic foliations to propagation using both the regional joints and gneissic foliations.

Thus, the effect of inherited structures can be described as faults exploiting two prolific fabrics: the gneissic foliations facilitate propagation of fault segments, and the joint sets to enable linkage between these segments. This relationship between faulting and the pervasive fabrics provides an explanation for the resulting morphology of the fault and for the geometry of the linage zones following the fault growth model of Trudgill & Cartwright (1994). Consequently, we suggest that pervasive upper crustal fabrics have allowed for the rapid development for fault segments according to the Walsh el at. (2003) model or to facilitate linkage according to the Trudgill & Cartwright (1994) model.

Model of Fault Growth

The pervasive inherited structures have modulated the stress field such that there was a rapid phase of tip propagation resulting in the development of three fault segments (BM1, 2, 3

and CN1, 2, 3). After which the fault segments experienced slower fault growth typical of the establishment of hard linkage (CN2-3 and BM 1-2). This evolution of dual phase fault growth has been reliant on the pervasive fabrics oriented both perpendicular and parallel to the minimum compressive stress. Therefore, we suggest that the inherited structures have allowed for the initial development of Walsh el at. (2003) type segments before transitioning to the Trudgill and Cartwright (1994) type fault segments. In areas with prolific upper crustal inherited structures, these structures are likely to exert an influence on the nucleation and propagation of faults. In this study, the diversity of inherited structures has allowed the faults to exploit them for either fault propagation or segment linkage.

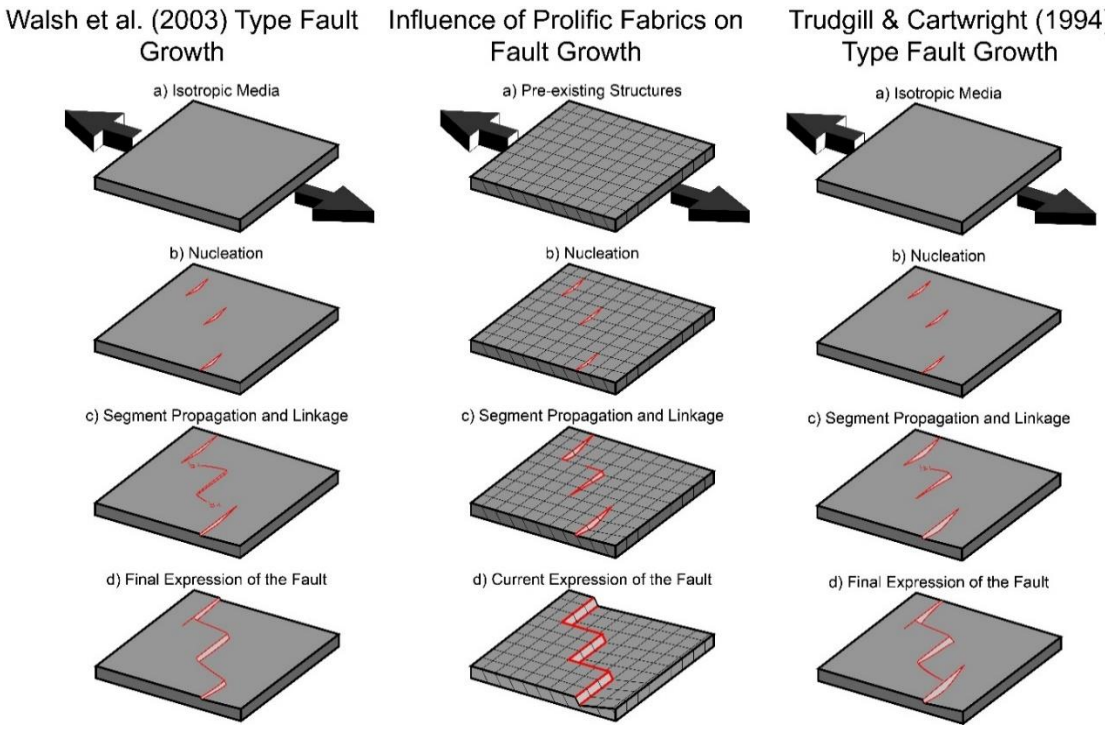

Figure 15: Comparison of fault growth models of Walsh et al. (2003), Trudgill & Cartwright (1994) and this study. The center model shows how inherited structures facilitate an intermediate type of segment growth and propagation. In this model the normal faulting is represented in red. The dark black lines perpendicular to extension represent pervasive upper crustal inherited structures well oriented for the development of normal faults. The lines parallel to extension are representative of pervasive upper crustal structures poorly oriented for extension but well oriented for linkage between segments. As the fault segments grow they use both inherited structures to facilitate rapid tip propagation with minimal displacement. Then the segments use the inherited structures parallel to extension to link between segments. This results in a continuous fault with a zig-zag morphology. The inherited structures allow the

fault to grow quickly as expected in the Walsh et al. (2003) model and the development of independent segments of the Trudgill & Cartwright (1994) model.

In our study area, the inherited structures control the location and orientation of the fault segments and the geometry of the linkage zones. We thus, propose a model to demonstrate this relationship. The conceptual model of Figure 15 shows how fault segments in a region of upper crustal pervasive preexisting fabrics are able to utilize the multiple structures during its growth and evolution. In our model the faults nucleate and propagate along the inherited structures perpendicular to the extension direction allowing for the rapid establishment of the fault segments expected by the Walsh et al. (2003) type fault growth and demonstrated by Patton (2006). Then the fault segments interact and become hard linked producing a continuous fault scarp representing Trudgill and Cartwright (1994) type fault growth. The resulting fault scarp reflects the geometry of the preexisting structures used in its development. This process reflects both the geometry of the fault morphology and the preexisting geology of our study area in Malawi.

Implications for Seismic Hazards

The northern segment (BM3) of the Bilila-Mtakataka Fault may be the causative fault for the 6.3 Mb 1989 Salima earthquake. This relationship is possible if the fault has a dip of 54° to 56° for the seismic event located at a 29.6-30.3 km deep with a lateral distance of 20-22 km to the fault scarp.

It is well known that the seismic potential is directly related to the geometry of the fault plane. Our study shows that the Chirobwe-Ncheu and Bilila-Mtakataka faults have 102 km and 159 km lengths measured along the fault scarp, respectively. For a region with known seismicity at 30-40 km depths these faults pose a major risk to the surrounding communities, if the faults where the rupture in a single event. However, the segmentation of the faults documented by this research show that the faults are only linked by soft linkage for the segments CN1-CN2 and

BM2-BM3. Thus, the seismic hazard is lessoned due to effective fault lengths of 78 km and 90 km for the Chirobwe-Ncheu and Bilila-Mtakataka faults respectively. Additionally, the faults are sub-perpendicular and thus, may simultaneously act to accommodate the strain, which would effectively reduce the seismic recurrence interval and the seismic hazard predicted for the region.

CHAPTER VI

CONCLUSION

We used SRTM-DEM and high resolution aeromagnetic data to map the fault segmentation and pervasive upper crustal fabrics in the region of the Chirobwe-Ncheu and Bilila-Mtakataka faults of the southern Malawi Rift. Our results suggest that the development and evolution of these > 100 km long faults are controlled in part by the orientation of the upper crustal pervasive preexisting fabrics. The segmentation and fault lengths established by this study have important implication for the seismic hazard of the region. In this area, the gneissic fabrics control the orientation and location of the fault segments where the foliation is perpendicular to extension. Furthermore, the combination of the regional joints and the gneissic fabrics control the linkage geometry. The pervasive preexisting upper crustal fabrics due to strain localization have resulted in the formation of two faults exhibiting characteristics of both the Walsh et al., (2003) and the Trudgill & Cartwright, (1994) fault growth models.

REFERENCES

Aanyu K, Koehn D (2011) Influence of pre-existing fabrics on fault kinematics and rift geometry of interacting segments: analogue models based on the Albertine Rift (Uganda), Western Branch-East African Rift System. Journal of African Earth Sciences 59:168–184.

Allmendinger, R. W., Cardozo, N., and Fisher, D., 2012, Structural geology algorithms: Vectors and tensors in structural geology: Cambridge University Press

Baranov, V. (1957). A new method for interpretation of aeromagnetic maps: pseudo-gravimetric anomalies. Geophysics, 22(2), 359-382.

Biggs, J., Nissen, E., Craig, T., Jackson, J., & Robinson, D. P. (2010). Breaking up the hanging wall of a rift-border fault: The 2009 Karonga earthquakes, Malawi. Geophysical Research Letters, 37(11).

Cardozo, N., & Allmendinger, R.W., (2013). Spherical projections with OSXStereonet: Computers & Geosciences, v. 51, p. 193 – 205

Chapola, L. S., & Kaphwiyo, C. E. (1992). The Malawi rift: geology, tectonics and seismicity. Tectonophysics, 209, 159-164.

Chattopadhyay, A., & Chakra, M. (2013). Influence of pre-existing pervasive fabrics on fault patterns during orthogonal and oblique rifting: an experimental approach. Marine and Petroleum Geology, 39(1), 74-91.

Chorowicz, J. (2005). The East African rift system. Journal of African Earth Sciences, 43(1-3), 379-410.

Chorowicz, J., & Sorlien, C. (1992). Oblique extensional tectonics in the Malawi Rift, Africa. Geological Society of America Bulletin, 104, 1015-1023.

Contreras, J., Anders, M., & Scholz, C. (2000). Growth of a normal fault system: observations from the Lake Malawi basin of the east African rift. Journal of Structural Geology, 22, 159-168.

Corti, G., van Wijk, J., Cloetingh, S., & Morley, C. K. (2007). Tectonic inheritance and continental rift architecture: Numerical and analogue models of the East African Rift system. Tectonics, 26(6).

Craig, T. J., Jackson, J. A., Priestley, K., & McKenzie, D. (2011). Earthquake distribution patterns in Africa: their relationship to variations in lithospheric and geological

structure, and their rheological implications. Geophysical Journal International, 185(1), 403-434.

Daly, M. C., Chorowicz, J., & Fairhead, J. D. (1989). Rift basin evolution in Africa: the influence of reactivated steep basement shear zones. Inversion Tectonics (44), 309-334.

Dawson, A. L., & Kirkpatrick, I. M. (1968). The geology of the Cape Maclear peninsula and Lower Bwanje valley. Malawi Geologic Bulletin No. 28.

Dawson, S. M., Laó-Dávila, D. A., Atekwana, E. A., & Abdelsalam, M. G. (2018). The influence of the Precambrian Mughese Shear Zone structures on strain accommodation in the northern Malawi Rift. Tectonophysics, 722, 53-68.

Delvaux, D., & Barth, A. (2010). African stress pattern from formal inversion of focal mechanism data. Tectonophysics, 482(1-4), 105-128.

Dunbar, J. A., & Sawyer, D. S. (1989). How preexisting weaknesses control the style of continental breakup. Journal of Geophysical Research: Solid Earth, 94(B6), 7278-7292.

Ebinger, C., Jackson, J., Foster, A., & Hayward, N. (1999). Extensional basin geometry and the elastic lithosphere. Philosophical Transactions of the Royal Society of

London A: Mathematical, Physical and Engineering Sciences, 357(1753), 741-765.

Ebinger, C. J. (1989). Tectonic development of the western branch of the East African rift system. Geological Society of America Bulletin, 101, 885-903.

Ebinger, C. J., Deino, A. L., Tesha, A. L., Becker, T., & Ring, U. (1993). Tectonic controls on rift basin morphology: evolution of the Northern Malawi (Nyasa) Rift. Journal of Geophysical Research: Solid Earth, 98(10), 17821-17836.

Ebinger, C. J., Rosendahl, B. R., & Reynolds, D. J. (1987). Tectonic model of the Malawi rift, Africa. Tectonophysics, 141, 215-235.

Fagereng, Å. (2013). Fault segmentation, deep rift earthquakes and crustal rheology: Insights from the 2009 Karonga sequence and seismicity in the Rukwa–Malawi rift zone. Tectonophysics, 601, 216-225.

Fossen, H., Odinsen, T., Faerseth, R. B., & Gabrielsen, R. H. (2000). Detachments and low-angle faults in the North Sea rift system. The Geological Society of London, 167, 105-131.

Fossen, H., & Rotevatn, A. (2016). Fault linkage and relay structures in extensional settings - A review. Earth-Science Reviews, 154, 14-28.

Henza, A. A., Withjack, M. O., & Schlische, R. W. (2011). How do the properties of a pre-existing normal-fault population influence fault development during a subsequent phase of extension?. Journal of Structural Geology, 33(9), 1312-1324.

Hodge, M., Biggs, J., Fagereng, A., & Mdala, H. (2018). Controls on early-rift geometry: new perspectives from the Bilila-Mtakataka fault, Malawi.

Hodge, M., Biggs, J., Goda, K., & Aspinall, W. (2015). Assessing infrequent large earthquakes using geomorphology and geodesy: the Malawi Rift. Natural Hazards, 76(3), 1781-1806.

Hodge, M., Fagereng, Å., & Biggs, J. (2018). The Role of Coseismic Coulomb Stress Changes in Shaping the Hard Link Between Normal Fault Segments. Journal of Geophysical Research: Solid Earth, 123(1), 797-814.

Holdsworth, R. E., Butler, C. A., & Roberts, A. M. (1997). The recognition of reactivation during continental deformation. Journal of the Geological Society, 154(1), 73-78.

Jackson, J., & Blenkinsop, T. (1997). The Bilila-Mtakataka fault in Malaŵi: An active, 100-km long, normal fault segment in thick seismogenic crust. Tectonics, 16(1), 137-150.

Katumwehe, A. B., Abdelsalam, M. G., & Atekwana, E. A. (2015). The role of pre-existing Precambrian structures in rift evolution: The Albertine and Rhino grabens, Uganda. Tectonophysics, 646, 117-129.

Kendall, J. M., & Lithgow-Bertelloni, C. (2016). Why is Africa rifting?. Geological Society, London, Special Publications, 420(1), 11-30.

Kim, Y. S., & Sanderson, D. J. (2005). The relationship between displacement and length of faults: a review. Earth-Science Reviews, 68(3-4), 317-334.

Kinabo, B. D., Hogan, J. P., Atekwana, E. A., Abdelsalam, M. G., & Modisi, M. P. (2008). Fault growth and propagation during incipient continental rifting: Insights from a combined aeromagnetic and Shuttle Radar Topography Mission digital elevation model investigation of the Okavango Rift Zone, northwest Botswana. Tectonics, 27(3).

Kolawole, F., Atekwana, E. A., Laó-Dávila, D. A., Abdelsalam, M. G., Chindandali, P. R., Salima, J., & Kalindekafe, L. (2018). Active deformation of Malawi Rift's North Basin hinge zone modulated by reactivation of pre-existing Precambrian shear zone fabric. Tectonics.

Koptev, A., Calais, E., Burov, E., Leroy, S., & Gerya, T. (2015). Dual continental rift systems generated by plume–lithosphere interaction. Nature Geoscience, 8(5), 388.

Laó-Dávila, D. A., Al-Salmi, H. S., Abdelsalam, M. G., & Atekwana, E. A. (2015). Hierarchical segmentation of the Malawi Rift: The influence of inherited lithospheric heterogeneity and kinematics in the evolution of continental rifts. Tectonics, 34(12), 2399-2417.

McConnell, R. B. (1972). Geological development of the rift system of eastern Africa. Geological Society of America Bulletin, 83(9), 2549-2572.

Miller, H. G., & Singh, V. (1994). Potential field tilt—a new concept for location of potential field sources. Journal of Applied Geophysics, 32(2-3), 213-217.

Misra, A. A., & Mukherjee, S. (2015). Tectonic inheritance in continental rifts and passive margins. Cham: Springer.

Morley, C. K., (1999) How successful are analogue models in addressing the influence of pre-existing fabrics on rift structure? Journal of Structural Geology 21:1267–1274.

Morley, C. K., (2010). Stress re-orientation along zones of weak fabrics in rifts: An explanation for pure extension in 'oblique' rift segments? Earth and Planetary Science Letters, 297(3-4), 667-673.

Morley, C. K., Haranya, C., Phoosongsee, W., Pongwapee, S., Kornsawan, A., & Wonganan, N. (2004). Activation of rift oblique and rift parallel pre-existing fabrics during extension and their effect on deformation style: examples from the rifts of Thailand. Journal of Structural Geology, 26(10), 1803-1829.

Mortimer, E. J., Paton, D. A., Scholz, C. A., & Strecker, M. R. (2016). Implications of structural inheritance in oblique rift zones for basin compartmentalization: Nkhata Basin, Malawi Rift (EARS). Marine and Petroleum Geology, 72, 110-121.

Muirhead, J. D., Kattenhorn, S. A., Lee, H., Mana, S., Turrin, B. D., Fischer, T. P., Kianji, G., Dindi, E., Stamps, D. S. (2016). Evolution of upper crustal faulting assisted by magmatic volatile release during early-stage continental rift development in the East African Rift. Geosphere, 12(6), 1670-1700.

Mukul, M., Srivastava, V., & Mukul, M. (2015). Analysis of the accuracy of shuttle radar topography mission (SRTM) height models using international global navigation satellite system service (IGS) network. Journal of Earth System Science, 124(6), 1343-1357.

Njinju, E. A. (2016). Crustal and sub-continental lithospheric mantle decoupling beneath the Malawi Rift (Doctoral dissertation, Oklahoma State University).

Oruç, B., & Selim, H. H. (2011). Interpretation of magnetic data in the Sinop area of Mid Black Sea, Turkey, using tilt derivative, Euler deconvolution, and discrete wavelet transform. Journal of Applied Geophysics, 74(4), 194-204.

Paton, D. A. (2006). Influence of crustal heterogeneity on normal fault dimensions and evolution: southern South Africa extensional system. Journal of Structural Geology, 28(5), 868-886.

Phillips, T. B., Jackson, C. A. L., Bell, R. E., Duffy, O. B., & Fossen, H. (2016). Reactivation of intrabasement structures during rifting: A case study from offshore southern Norway. Journal of Structural Geology, 91, 54-73.

Piper, D. P. (1989). Lineament analysis of the environs of the Malawi rift and the influence of pre-existing structures on rift morphology. Journal of African Earth Sciences, 9, 579-587.

Reed, C. A., Liu, K. H., Chindandali, P., Massingue, B., Mdala, H., Mutamina, D., Yu, Y., & Gao, S. S. (2016). Passive rifting of thick lithosphere in the southern East African Rift: Evidence from mantle transition zone discontinuity topography. Journal of Geophysical Research: Solid Earth, 121(11), 8068-8079.

Ring, U. (1994). The influence of preexisting structure on the evolution of the Cenozoic Malawi rift (East African rift system). Tectonics, 13(2), 313-326.

Rodriguez, E., Morris, C. S., & Belz, J. E. (2006). A global assessment of the SRTM performance. Photogrammetric Engineering & Remote Sensing, 72(3), 249-260.

Sarafian, E., Evans, R. L., Abdelsalam, M. G., Atekwana, E., Elsenbeck, J., Jones, A. G., & Chikambwe, E. (2018). Imaging Precambrian lithospheric structure in Zambia using electromagnetic methods. Gondwana Research, 54, 38-49.

Saria, E., Calais, E., Stamps, D. S., Delvaux, D., & Hartnady, C. J. H. (2014). Present-day kinematics of the East African Rift. Journal of Geophysical Research: Solid Earth, 119(4), 3584-3600.

Specht, T. D., & Rosendahl, B. R. (1989). Architecture of the Lake Malawi rift, East Africa. African Earth Sciences, 8, 355-382.

Stamps, D. S., Saria, E., & Kreemer, C. (2018). A Geodetic Strain Rate Model for the East African Rift System. Scientific reports, 8(1), 732.

Thatcher, E. C. (1969). The geology of the Dedza area. Malawi Geologic Bulletin No. 29.

Thurston, J. B., & Smith, R. S. (1997). Automatic conversion of magnetic data to depth, dip, and susceptibility contrast using the SPI (TM) method. Geophysics, 62(3), 807-813.

Trudgill, B., & Cartwright, J. (1994). Relay-ramp forms and normal-fault linkages, Canyonlands National Park, Utah. Geological Society of America Bulletin, 106, 1143-1157.

Van Der Beek, P., Mbede, E., Andriessen, P., & Delvaux, D. (1998). Denudation history of the Malawi and Rukwa Rift flanks (East African Rift System) from apatite fission track thermochronology. Journal of African Earth Sciences, 26(3), 363-385.

Versfelt, J., & Rosendahl, B. R. (1989). Relationships between pre-rift structure and rift architecture in lakes Tanganyika and Malawi, East Africa. Nature, 337, 354-357.

Walsh, J. J., Bailey, W. R., Childs, C., Nicol, A., & Bonson, C. G. (2003). Formation of segmented normal faults: a 3-D perspective. Journal of Structural Geology, 25(8), 1251-1262.

Walshaw, R.D. (1965). The geology of the Ncheu-Balaka area. Malawi Geologic Bulletin. No. 19.

Walter, M. J. (1972). The geology of the Slima-Mvera Mission area. Malawi Geologic Bulletin No. 30.

Yang, Z., & Chen, W. P. (2010). Earthquakes along the East African Rift System: A multiscale, system-wide perspective. Journal of Geophysical Research: Solid Earth, 115(B12).

Zwaan, F., & Schreurs, G. (2017). How oblique extension and structural inheritance influence rift segment interaction: Insights from 4D analog models. Interpretation, 5(1), SD119-SD138.

Zwaan, F., Schreurs, G., Naliboff, J., & Buiter, S. J. (2016). Insights into the effects of oblique extension on continental rift interaction from 3D analogue and numerical models. Tectonophysics, 693, 239-260.

APPENDICES

Data Set	Sample Size	Mean Direction	Mean Length	Circular Variance	kappa
Region C SRTM Lineaments	179	327.1° ± 45.0°	0.0517	0.9483	0.1001
Region B SRTM Lineaments	313	286.1° ± 6.5°	0.4439	0.5561	0.9821
Region A SRTM Lineaments	99	347.7° ± 17.2°	0.2376	0.7624	0.4727
Region C Aeromagnetic Lineaments	46	030.9° ± 6.8°	0.7213	0.2787	2.1436
Region B Aeromagnetic Lineaments	28	325.4° ± 14.8°	0.4847	0.5153	1.0979
Region A Aeromagnetic Lineaments	69	328.9° ± 11.6°	0.4043	0.5957	0.7213
Region C Chirobwe-Ncheu	149	010.4° ± 3.1°	0.8005	0.1995	2.8713
Region B Chirobwe-Ncheu	1031	343.4° ± 0.9°	0.8941	0.1059	4.8587
Region A Chirobwe-Ncheu	1349	347.4° ± 0.9°	0.855	0.145	3.6804
Region C Bilila-Mtakataka	1879	335.4° ± 0.8°	0.82	0.18	3.1426
Region B Bilila-Mtakataka	906	340.8° ± 0.7°	0.9401	0.599	8.6104
Region A Bilila-Mtakataka	1388	319.6° ± 0.7°	0.8999	0.1001	4.8587

Table 1: The statistical information for regions A, B, and C of the SRTM and aeromagnetic derived data and the fault strike data.

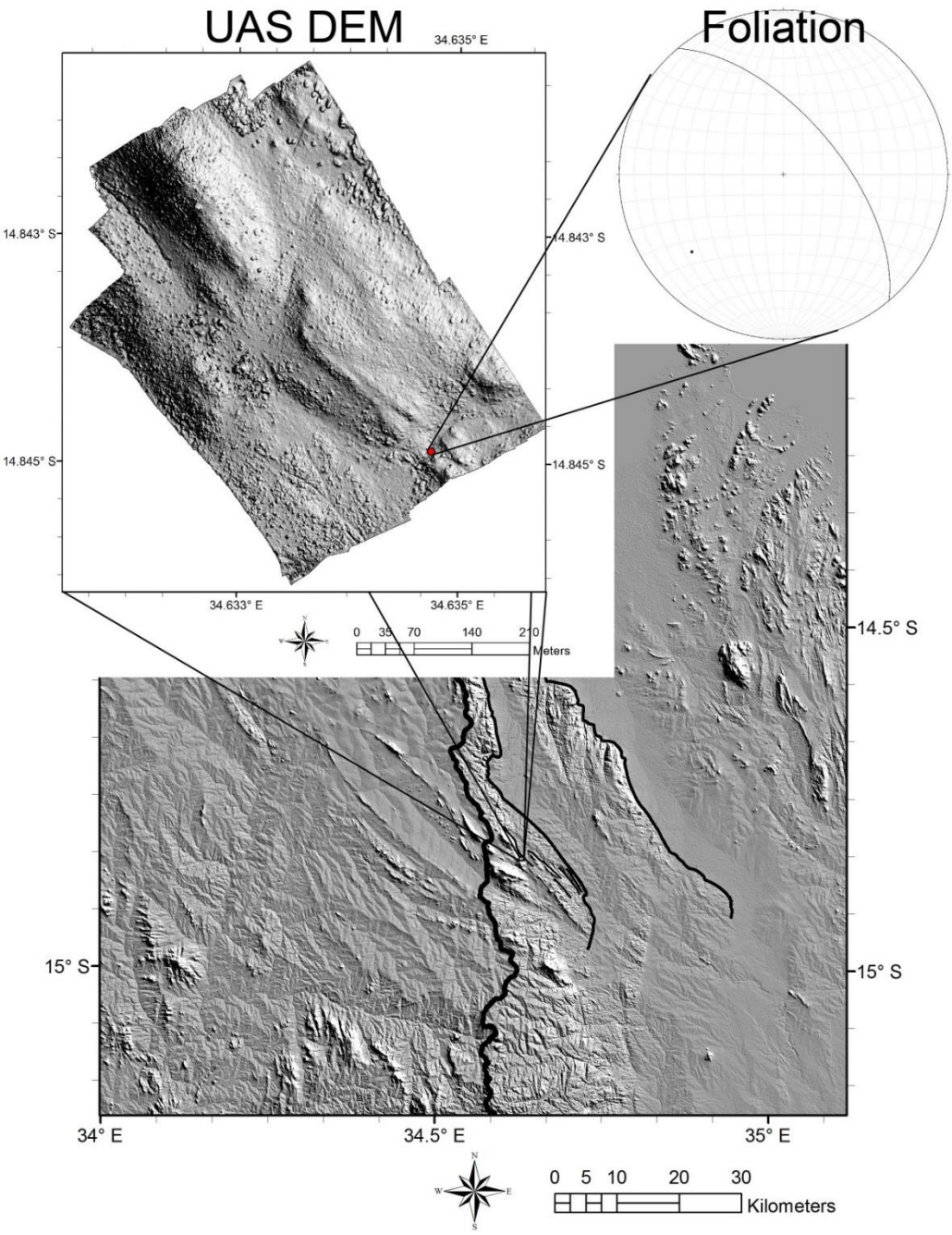

Begin

Figure A1: a map showing a high resolution DEM generated using Structure form Motion techniques. The ridge follows the same strike as the foliations mapped by our meso-scale field work.

VITA

Steven Grant Johnson

Candidate for the Degree of

Master of Science

Thesis: THE INFLUENCE OF INHERITED STRUCUTRES ON SEGMENTATION AND LINKAGE OF TWO SUBPARALLEL FAULTS IN SOUTHERN MALAWI

Major Field: GEOLOGY

Biographical:

Education:
Completed the requirements for the Master of Science in your major at Oklahoma State University, Stillwater, Oklahoma in May, 2018.

Completed the requirements for the Bachelor of Science in Geology at Oklahoma State University, Stillwater, Oklahoma USA in 2016.

Experience:
International research with Dr. Laó Dávila in Malawi, Africa July - Aug. 2017

- Collecting structural data of faults, folds, dikes, and joints
- Generated electrical resistivity profiles using the IRIS Syscal Pro
- Conducted gravity and magnetic profiles using Geometrix G858 magnetometer and Syntrix cg5 gravimeter
- Obtaining photos with a UAS to generate 3-D models using the Structure from Motion methodology

Field experience with Dr. Laó Dávila in Puerto Rico, USA March 2016

- Gathering structural data and making field reports to better understand the tectonics of Puerto Rico

Lab Assistant with Dr. Donoghue at Oklahoma State University June - July 2015

- Investigated partial sizes of sediment size using a Cilas 1180
- Gamma ray emission spectrometry for sample dating

Professional Memberships:
American Geophysical Union (AGU)
American Association of Petroleum Geologist (AAPG)
Geological Society of America (GSA)
Society of Exploration Geophysicists (SEG)